

Radiopharmaceutical tracers for cardiac imaging

Osamu Manabe, MD, PhD,^a Tatsuya Kikuchi, PhD,^b Arthur J. H. A. Scholte, MD, PhD,^c Mohammed El Mahdiui, MD,^c Ryuichi Nishii, MD, PhD,^d Ming-Rong Zhang, PhD,^b Eriko Suzuki, LT,^a and Keiichiro Yoshinaga, MD, PhD, FACC, FASNC^d

^a Department of Nuclear Medicine, Hokkaido University Graduate School of Medicine, Sapporo, Japan

^b Department of Radiopharmaceutical Development, National Institutes for Quantum and Radiological Science and Technology, National Institute of Radiological Sciences, Chiba, Japan

^c Department of Cardiology, Leiden University Medical Center, Leiden, The Netherlands

^d Diagnostic and Therapeutic Nuclear Medicine, National Institutes for Quantum and Radiological Science and Technology, National Institute of Radiological Sciences, Chiba, Japan

Received Nov 3, 2017; accepted Nov 5, 2017

doi:10.1007/s12350-017-1131-5

Cardiovascular disease (CVD) is the leading cause of death and disease burden worldwide. Nuclear myocardial perfusion imaging with either single-photon emission computed tomography or positron emission tomography has been used extensively to perform diagnosis, monitor therapies, and predict cardiovascular events. Several radiopharmaceutical tracers have recently been developed to evaluate CVD by targeting myocardial perfusion, metabolism, innervation, and inflammation. This article reviews old and newer used in nuclear cardiac imaging. (J Nucl Cardiol 2018;25:1204–36.)

Key Words: Cardiovascular disease • positron emission tomography • radiopharmaceutical • single-photon emission computed tomography

Electronic supplementary material The online version of this article (<https://doi.org/10.1007/s12350-017-1131-5>) contains supplementary material, which is available to authorized users.

The authors of this article have provided a PowerPoint file, available for download at SpringerLink, which summarises the contents of the paper and is free for re-use at meetings and presentations. Search for the article DOI on SpringerLink.com.

Reprint requests: Keiichiro Yoshinaga, MD, PhD, FACC, FASNC, Diagnostic and Therapeutic Nuclear Medicine, National Institutes for Quantum and Radiological Science and Technology, National Institute of Radiological Sciences, 4-9-1 Anagawa, Inage-Ku, Chiba 263-8555, Japan; yoshinaga.keiichiro@qst.go.jp

1071-3581/\$34.00

Copyright © 2017 The Author(s). This article is an open access publication

Abbreviations	
¹¹ C-CGP12177	(<i>S</i>)-4-(3-((1,1-dimethylethyl)amino)-2-hydroxypropoxy)-[<i>car-bonyl</i> - ¹¹ C]1,3-dihydro-2 <i>H</i> -benzimidazol-2-one
¹¹ C-CGP12388	(<i>S</i>)-4-(3-(2'-[<i>methine</i> - ¹¹ C]isopropylamino)-2-hydroxypropoxy)-2 <i>H</i> -benzimidazol-2-one
¹¹ C-HED	[¹¹ C]hydroxyephedrine
¹¹ C-PK11195	1-(2-chlorophenyl)- <i>N</i> -[¹¹ C]methyl- <i>N</i> -1(1-methylpropyl)-3-isoquinolinecarboxamide
¹²³ I-BMIPP	β-methyl- <i>p</i> -[¹²³ I]iodophenylpentadecanoic acid
¹²³ I-IPPA	<i>p</i> - <i>o</i> -[¹²³ I]iodophenylpentadecanoic acid
¹²³ I-MIBG	<i>m</i> -[¹²³ I]iodobenzylguanidine
¹³ N-NH ₃	[¹³ N]ammonia
¹⁵ O-H ₂ O	[¹⁵ O]water
¹⁸ F-FDG	2-[¹⁸ F]fluorodeoxyglucose
¹⁸ F-FEDAC	<i>N</i> -benzyl- <i>N</i> -methyl-2-[7,8-dihydro-7-(2-[¹⁸ F]fluoroethyl)-8-oxo-2-phenyl-9 <i>H</i> -purin-9-yl]acetamide
¹⁸ F-FLT	[¹⁸ F]fluorothymidine
¹⁸ F-FMISO	[¹⁸ F]fluoromisonidazole
¹⁸ F-FTHA	[¹⁸ F]fluoro-6-thia-heptadecanoic acid
¹⁸ F-NaF	Sodium [¹⁸ F]fluoride
⁶⁸ Ga-DOTANOC	⁶⁸ Ga-complex with 1,4,7,10-tetraazacyclododecane-1,4,7,10-tetraacetic acid-1- <i>NaI</i> ³ -octreotide
⁶⁸ Ga-DOTATATE	⁶⁸ Ga-complex with 1,4,7,10-tetraazacyclododecane-1,4,7,10-tetraacetic acid- <i>D</i> -Phe ¹ -Tyr ³ -octreotate
⁶⁸ Ga-DOTATOC	⁶⁸ Ga-complex with 1,4,7,10-tetraazacyclododecane-1,4,7,10-tetraacetic acid- <i>D</i> -Phe ¹ -Tyr ³ -octreotide
^{99m} Tc-MIBI	^{99m} Tc-sestamibi
acetyl-CoA	Acetyl coenzyme A
Ach	Acetylcholine
ATP	Adenosine triphosphate
CVD	Cardiovascular disease
CMR	Cardiac magnetic resonance
COMT	Catechol- <i>O</i> -methyltransferase
ECG	Electrocardiographically
FDA	Food and Drug Administration

FFA	Free fatty acid
HFpEF	Heart failure with preserved ejection fraction
HF	Heart failure
HMR	Heart-to-mediastinum ratio
HR	Heart rate
ICD	Indication for cardioverter-defibrillator implantation
LMI1195	<i>N</i> -(3-bromo-4-(3-[¹⁸ F]fluoropropoxy)benzyl)-guanidine
LV	Left ventricular
MAO	Monoamine oxidase
MBF	Myocardial blood flow
MPI	Myocardial perfusion imaging
NE	Norepinephrine
PAP	Pulmonary artery pressure
PET	Positron emission tomography
PH	Pulmonary hypertension
PS	Phosphatidylserine
RV	Right ventricle
SPECT	Single-photon emission computed tomography
TCA	Tricarboxylic acid
TSPO	Translocator protein 18kDa
VMAT	Vesicular monoamine transporter
WBC	White blood cell
β-AR	β-adrenergic receptor

See related editorial, pp. 1242–1246

INTRODUCTION

Cardiovascular disease (CVD) is the leading cause of death and disease burden around the world.¹ Advances in single-photon emission computed tomography (SPECT) and positron emission tomography (PET), which allow for non-invasive imaging, are vastly improving the evaluation of myocardial perfusion and function.^{2,3} Nuclear cardiac imaging is useful to perform diagnosis and risk assessment and to monitor the impact of therapies through serial imaging. Several radiopharmaceutical tracers are used in nuclear cardiology imaging to target perfusion, metabolism, innervation, and inflammatory conditions. Nuclear imaging tests are suitable for almost all patients given the low possibilities of side effects from radiopharmaceutical tracers other than minimal radiation exposure. In this article, we will review SPECT and PET tracers used in assessing CVD.

Table 1. Classification of cardiac imaging tracers by characteristics

Characteristics	Tracer
Inorganic tracers	$^{13}\text{N-NH}_3$
	$^{15}\text{O-H}_2\text{O}$
Radiometal ions	$^{201}\text{Tl}^+$
	$^{82}\text{Rb}^+$
	$^{67}\text{Ga}^{3+}$
	$^{18}\text{F}^-$
Small organic tracers	^{11}C -acetic acid
	^{11}C -palmitic acid
	^{123}I -IPPA
	^{18}F -FDG
	^{123}I -BMIPP
	^{18}F -FTHA
	^{11}C -epinephrine
	^{18}F -fluorodopamine
	Derivatives of guanethidine, metaraminol, and vesamicol
	Neuroreceptor ligands such as prazosin (α -blocker), carazolol (β -blocker) derivative, β -agonists (CGP12177 and CGP12388), and quinuclidinyl benzilate (anticholinergic compound)
	^{11}C -PK11195
	^{18}F -FEDAC
Radiometal complex tracers	$^{99\text{m}}\text{Tc}$ -sestamibi
	$^{99\text{m}}\text{Tc}$ -tetrofosmin
	Somatostatin analogs and annexin V tagged with ^{64}Cu , ^{68}Ga , or $^{99\text{m}}\text{Tc}$
	$^{99\text{m}}\text{Tc}$ -tagged annexin A5
	^{111}In -oxine
	$^{99\text{m}}\text{Tc}$ -HMPAO

**TRACERS USED FOR CARDIAC IMAGING
(TABLE 1)**

Inorganic Tracers

Inorganic compounds ^{13}N -ammonia ($^{13}\text{N-NH}_3$) and ^{15}O -water ($^{15}\text{O-H}_2\text{O}$) have been used for cardiac perfusion imaging.⁴ Both tracers are labeled with short-lived positron emitters (^{13}N : 10 minute; ^{15}O : 2 minute), which are therefore produced with an onsite cyclotron. $^{15}\text{O-H}_2\text{O}$ is freely diffused into cardiomyocytes. In contrast, the uptake mechanism of $^{13}\text{N-NH}_3$ is unclear.⁵ Almost all ammonia molecules in the blood would be protonated to form NH_4^+ because of its pKa (9.3 at 25 °C). The ammonium cation would barely penetrate cell membranes to enter cardiomyocytes.

Radiometal Ions

In addition to these inorganic compounds, several radiometal ions have been used as cardiac imaging tracers, especially in myocardial perfusion imaging.

Initially, the monovalent cation of potassium-43 ($^{43}\text{K}^+$), a γ -emitter, was used for imaging of myocardial perfusion.⁶ However, the main gamma energy of this radionuclide (0.37 and 0.67 MeV) is somewhat too high for SPECT imaging. Also ^{43}K has a relatively long half-life (22 hours) and emits relatively high-energy β -particles [300 keV (mean)]. K^+ is actively transported into the myocyte by the cell membrane via Na^+/K^+ pumps. Therefore, other monovalent cations that emit γ -rays suitable for SPECT imaging were sought. The ionic radius of the candidate should be comparable to that of K^+ (138 pm) to be a substrate of a Na^+/K^+ pump. The monovalent cation of thallium-201 ($^{201}\text{Tl}^+$, ionic radius; 150 pm) fulfills these requirements and has been widely used for diagnosis of coronary artery disease (CAD). Although ^{201}Tl emits γ -rays of 135 and 167 keV, abundantly emitted characteristic x-rays (69 to 80 keV) are used for imaging.

A positron emitter, rubidium-82 (^{82}Rb), has an ionic radius (152 pm) comparable to that of K^+ in its monovalent cationic form ($^{82}\text{Rb}^+$) and belongs to the

same family as K (alkaline metals). The kinetics of Rb^+ are similar to those of K^+ , and therefore, $^{82}\text{Rb}^+$ has been widely used as a perfusion imaging tracer with PET in the United States (USA).⁸ In addition, the use of a positron-emitting isotope of K, potassium-38, has been also reported.⁹ Trivalent cations of gallium-67 ($^{67}\text{Ga}^{3+}$), a γ -emitter, have been used to detect inflammatory lesions. Ga^{3+} binds to ferric iron (Fe^{3+})-binding proteins such as transferrin and lactoferrin which are accumulated in inflammatory lesions.¹⁰ Besides cationic radionuclides, a monovalent anion of fluorine-18 ($^{18}\text{F}^-$) that is used for bone imaging has been used for imaging calcification lesions with PET.¹¹

Small Organic Tracers

Tracers of radiolabeled small organic compounds are used for imaging metabolism, synaptic function, and inflammation. In metabolic imaging, radiolabeled biomolecules and their derivatives are used. Biomolecules, acetic acid, and palmitic acid, substrates of oxygen metabolism and fatty acid metabolism, have been labeled with carbon-11 (^{11}C -acetic acid and ^{11}C -palmitic acid) and used for the assessment of respective myocardial metabolism.¹² Iodophenylpentadecanoic acid labeled with iodine-123, (^{123}I -IPPA) is also a substrate of fatty acid metabolism. For labeling with ^{123}I , a phenyl group was incorporated into the structure of palmitic acid. In the development of tracers, derivatization of a biomolecule is often performed to obtain a compound that is metabolized by a certain metabolic step without undergoing further metabolism. 2- ^{18}F fluorodeoxyglucose (^{18}F -FDG) is one such derivative of glucose. β -methyl- p - ^{123}I iodophenylpentadecanoic acid (^{123}I -BMIPP) and ^{18}F fluoro-6-thia-heptadecanoic acid (^{18}F -FTHA) introduce a methyl group and thioether in the alkyl chain, respectively, to terminate β -oxidation in the course of fatty acid metabolism.

In presynaptic cardiac imaging, a radiolabeled catecholamine and its derivative are also used as a tracer. ^{11}C -labeled epinephrine and ^{18}F -labeled fluorodopamine (^{18}F -fluorodopamine) have been used to image the presynaptic sympathetic nervous system.¹³ In addition to biomolecules, xenobiotics including therapeutics are radiolabeled and used as tracers. Derivatives of guanethidine, metaraminol, and vesamicol are used for presynaptic imaging, and neuroreceptor ligands such as prazosin (α -blocker), carazolol (β -blocker) derivative, β -agonists CGP12177 and CGP12388, and quinuclidinyl benzilate (anticholinergic compound) derivatives are used for neuroreceptor imaging (Table 4).¹³

Radiolabeled receptor ligands for translocator protein 18 kDa (TSPO), peripheral-type benzodiazepine receptors, have also been used to image inflammation.

TSPO is highly expressed in activated cells of the mononuclear phagocyte.¹⁴

Radiometal Complex Tracers

Some tracers used in nuclear cardiology are radiometal complexes containing copper-64 (^{64}Cu), gallium-68 (^{68}Ga), or technetium-99m ($^{99\text{m}}\text{Tc}$). They are classified into two groups. One contains those complexes that are used as tracers on their own. $^{99\text{m}}\text{Tc}$ is used to form a complex with six methoxyisobutylisonitrile ($^{99\text{m}}\text{Tc}$ -sestamibi) and two 1,2-bis(di(2-ethoxyethyl)phosphino) ethane ($^{99\text{m}}\text{Tc}$ -tetrofosmin), which have been used for myocardial perfusion imaging. Their bulky structures contribute to reducing protein binding in the blood through steric hindrance. These tracers are positively charged (monovalent) but lipophilic. Therefore, they can be diffused into myocytes.

The other group includes complexes used as tags for peptides and proteins. Somatostatin analogs and annexin V tagged with ^{64}Cu , ^{68}Ga , or $^{99\text{m}}\text{Tc}$ have been used for imaging symptomatic carotid atherosclerosis.¹⁵ ^{64}Cu or ^{68}Ga -tagged somatostatin analogs bind to somatostatin receptor subtype-2, which is upregulated in macrophages. $^{99\text{m}}\text{Tc}$ -tagged annexin A5 binds to phosphatidylserine, which is externalized in apoptotic cells.

White blood cells enclosing radiometals, which are used for imaging infectious lesions, are prepared using lipophilic radiometal complexes. Indium-111 (^{111}In) complexed with 8-hydroxyquinolines (^{111}In -oxine) and $^{99\text{m}}\text{Tc}$ complexed with exametazime ($^{99\text{m}}\text{Tc}$ -HMPAO) are diffused into the leucocyte. The subsequent dissociation of ligands results in enclosure of these radiometals in the cell.

RADIOTRACERS CATEGORIZED BY USE

Perfusion Imaging

Myocardial blood flow (MBF) is supplied by coronary arteries to preserve adequate myocardial oxygen supply. At rest, coronary artery stenosis must exceed 85% to 90% of luminal diameter before there is a significant decrease of MBF. In contrast, maximal coronary flow has been shown to be reduced with stenosis of 45% to 50% under stress condition.¹⁶ Myocardial perfusion images during stress and rest are compared to detect the stress-induced ischemic change or myocardial injury (Figure 1).^{17,18} Several perfusion tracers are used to assess coronary artery disease (CAD) (Table 2, Figure 2).^{17,19–22}

SPECT tracers for perfusion imaging. Thallium-201 (^{201}Tl), technetium-99m ($^{99\text{m}}\text{Tc}$)-sestamibi,

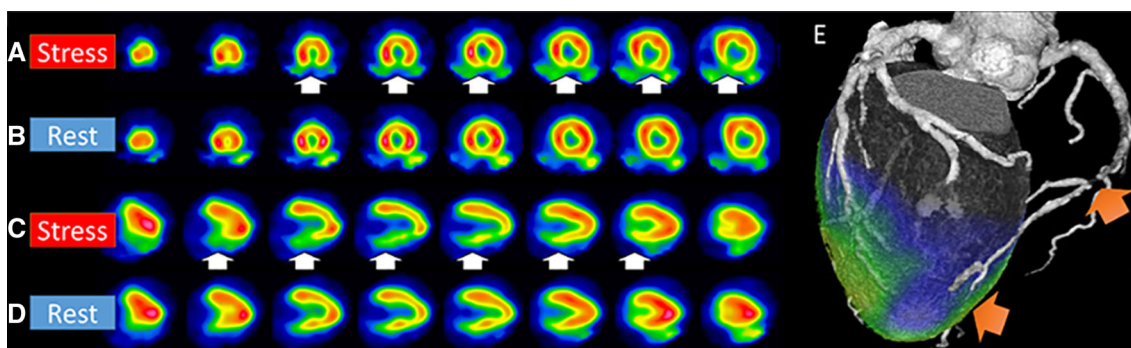


Figure 1. Myocardial perfusion images. Perfusion images of short-axis image at stress (A) and rest (B), vertical long-axis image at stress (C) and rest (D) using ^{99m}Tc -product, and fused image of stress perfusion and CT coronary angiography (CTCA; E) are displayed. Severe perfusion reduction is detected in the inferior wall at stress (white arrows). Fill-in is seen at rest indicating stress-induced ischemia in the right coronary artery (RCA). CTCA revealed significant stenosis in the RCA (orange arrows).

and ^{99m}Tc -tetrofosmin are available for SPECT myocardial perfusion imaging (MPI).

^{99m}Tc -labeled myocardial perfusion tracers. Thallium-201

^{201}Tl , introduced in the 1970 s, was the first SPECT MPI tracer available in a clinical setting.²³ In 1975, Wackers et al. reported on the imaging of acute myocardial infarction with ^{201}Tl .²⁴ ^{201}Tl is produced in a cyclotron and has a relatively long half-life (73 hours), and therefore requires lower injection doses to minimize radiation exposure. ^{201}Tl is a potassium analog and is transported into the myocyte via cell membrane Na^+/K^+ pumps during the first transit in proportion to regional MBF.

^{201}Tl emits low-energy photons (71 to 80 keV), therefore requiring longer imaging acquisition times and resulting in limited image quality due to absorption and photon scattering especially in obese patients. Biodistribution of ^{201}Tl is generally proportional to organ blood flow. Injected ^{201}Tl is rapidly cleared from the blood with maximal concentration by normal myocardium (5% to 8% remains in the blood at 5 minutes). The whole-body retention curve can be represented by a biexponential curve. ^{201}Tl is excreted slowly in both feces and urine. Approximately 4% to 8% of the administered dose is excreted in the urine in the first 24 hours.^{25,26} Lung uptake of ^{201}Tl is generally low. An increased lung uptake is known to be associated with greater segmental myocardial perfusion abnormality, increased severity and extent of CAD, and subsequent adverse cardiac events.²⁷

Whole-body radiation exposure after an injection (2 to 4 mCi) is up to ~ 25 mSv.^{28,29}

^{201}Tl has a higher extraction coefficient than do ^{99m}Tc -labeled perfusion tracers (Figure 3). The higher extraction fraction may be an advantage for MBF quantification.³⁰

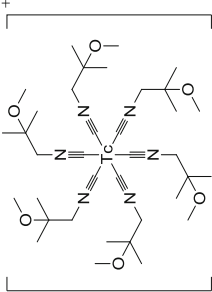
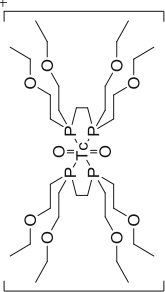
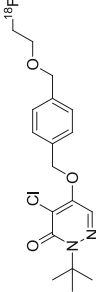
Stress images are acquired 5 to 15 minutes after tracer injection in order to avoid the “upward creep” phenomenon due to rapid respiration if the stress is produced through exercise. Redistribution images are acquired 2 to 4 hours after initial injection. Differential washout rates of normal regions (with faster washout) vs regions with ischemic segments (slower washout) contribute to the redistribution or normalization of the abnormal regions in delayed images.

^{99m}Tc -labeled myocardial perfusion tracers. ^{99m}Tc is a generator-produced agent eluted from molybdenum-99 (^{99}Mo). Despite its initial Food and Drug Administration (FDA) approval, ^{99m}Tc -teboroxime is far less commonly used due to the excessive initial uptake in the myocardium and rapid washout.^{31,32} ^{99m}Tc -sestamibi and ^{99m}Tc -tetrofosmin have had widespread clinical use. The first use of ^{99m}Tc -tetrofosmin for humans was reported in 1993 as part of a phase I clinical trial.³³ Injected ^{99m}Tc -labeled perfusion tracer distributes in the myocardium according to regional myocardial perfusion. Its uptake by myocardium is related to the presence of intact mitochondria.³⁴

Because its half-life is 6 hours, the administered dose is relatively larger and the radiation exposure is lower respectively than those associated with ^{201}Tl .²⁹ The peak energy level of γ -rays from ^{99m}Tc is about 140 keV, which is suitable for γ -camera imaging and electrocardiographically (ECG) gated myocardial perfusion SPECT.

^{99m}Tc -sestamibi is rapidly cleared from blood after intravenous administration. Lung uptake is generally

Table 2. Tracers for perfusion imaging

Tracer	Chemical structure*	Type of tracer	Production	Half-life	Positron range (mm)	Scan duration (rest and stress)	Intravenously administered activity (MBq)	Effective dose (mSv/MBq)	Approval year			
									FDA	Europe	Japan	
SPECT												
$^{201}\text{Tl}^+$		Metal cation	Cyclotron	73 h	-	4-h	74-148	0.23	1977	1980**	1991	
$^{99\text{m}}\text{Tc}$ -sestamibi		Metal complex	Generator	6 h	-	4-h or 2-days	740-1480	0.0085	1990	1987**	1993	
$^{99\text{m}}\text{Tc}$ -tetrofosmin		Metal complex	Generator	6 h	-	4-h or 2 days	740-1480	0.0067	1996	1993**	1996	
$^{99\text{m}}\text{Tc}$ -teboroxime									1990	-	-	
PET												
$^{82}\text{Rb}^+$		Metal cation	Generator	76 s	8.6	30-min	370-740	0.0048	1989	-	-	
^{13}N -ammonia		Inorganic compound	Cyclotron	9.96 min	2.53	1.5-h	370-740	0.0022	2007	-	2012	
^{15}O -water		Inorganic compound	Cyclotron	2.04 min	4.14	30-min	370-740	0.0011	-	-	-	
^{18}F -flurpiridaz		Organic compound	Cyclotron	109.8 min	1.03	1.5-h or 2 days	222-370	0.019	-	-	-	

* The mass number of $^{99\text{m}}\text{Tc}$ was omitted

** EURD List Juli 2017: http://www.ema.europa.eu/docs/en_GB/document_library/Other/2012/10/WC500133159.xls

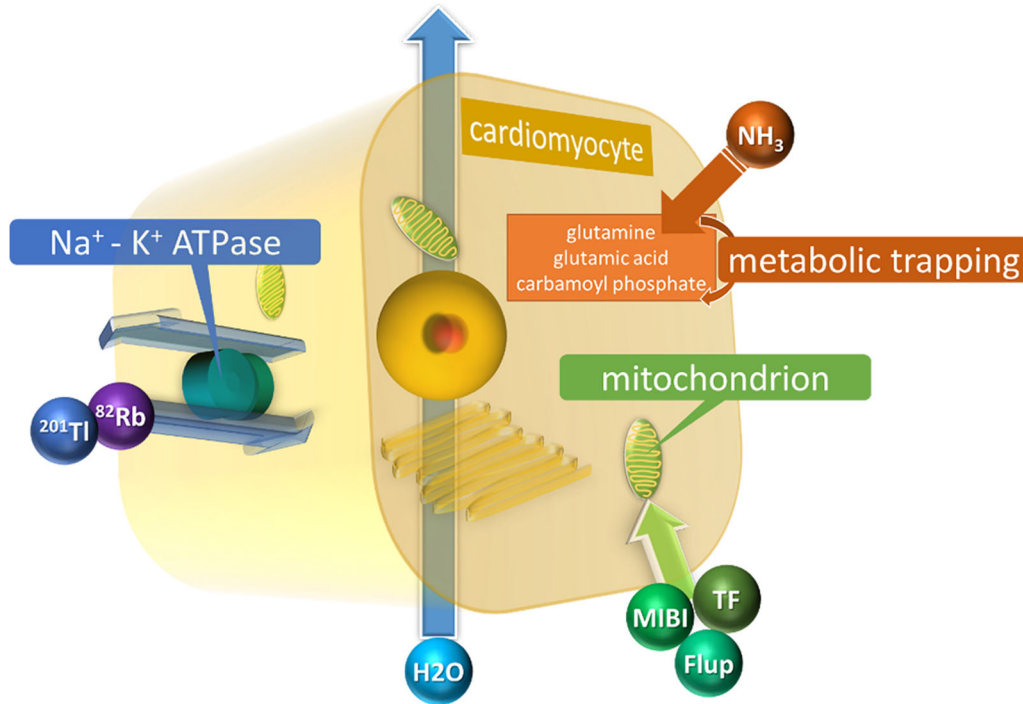


Figure 2. Schematic representation of tracers for assessing myocardial perfusion ^{201}Tl and ^{82}Rb are potassium analogs and are transported into the myocyte by cell membrane Na^+/K^+ pumps. Injected uptake of $^{99\text{m}}\text{Tc}$ -sestamibi, $^{99\text{m}}\text{Tc}$ -tetrofosmin, and ^{18}F -flurpiridaz in the myocardium is related to the presence of intact mitochondria. The uptake mechanism of ^{13}N - NH_3 is unclear. After being taken into the myocyte, ^{13}N - NH_3 underwent metabolic trapping with the conversion of NH_3 to glutamine, glutamic acid, and carbamoyl phosphate. ^{15}O - H_2O is metabolically inert and freely diffusible tracer.

low. However, marked accumulation is present in liver and spleen at resting condition during the first 60 minutes after injection. After an injection with exercise stress, substantially less uptake is observed in the liver and spleen with excellent visualization of heart.³⁵ $^{99\text{m}}\text{Tc}$ -tetrofosmin is rapidly cleared from the blood (< 5% remains in blood by 10 minutes) after intravenous administration. Uptake in myocardium is approximately 1.2% with minimal redistribution, and approximately 1% at 2 hours. Clearance from liver is quick (< 4.5% remains by 60 minutes) and lung uptake is also rapidly reduced.^{33,36,37} Myocardial uptake of $^{99\text{m}}\text{Tc}$ -tetrofosmin is higher from 5 to 60 minutes than is that for $^{99\text{m}}\text{Tc}$ -sestamibi. The biological half-life of $^{99\text{m}}\text{Tc}$ -tetrofosmin in normal myocardium and liver is significantly shorter than that of $^{99\text{m}}\text{Tc}$ -sestamibi. Heart-to-lung ratios for $^{99\text{m}}\text{Tc}$ -tetrofosmin and $^{99\text{m}}\text{Tc}$ -sestamibi are similar, whereas heart-to-liver ratios for $^{99\text{m}}\text{Tc}$ -tetrofosmin are significantly higher from 30 to 60 minutes post injection compared to those for $^{99\text{m}}\text{Tc}$ -sestamibi.^{37,38}

Total whole-body radiation after a typical injection dose (10 to 25 mCi) is ~ 10.6 mSv for $^{99\text{m}}\text{Tc}$ -tetrofosmin and 12.0 mSv for $^{99\text{m}}\text{Tc}$ -sestamibi.²⁸

Separate stress and rest injections are required for the detection of stress-induced ischemia due to its slow clearance from myocytes. Both $^{99\text{m}}\text{Tc}$ -sestamibi and $^{99\text{m}}\text{Tc}$ -tetrofosmin have lower extraction coefficients than does ^{201}Tl (Figure 3).³⁹ Recent SPECT systems allow the quantification of MBF from dynamic tracer imaging due to the improved sensitivity and temporal resolution.^{40,41}

PET tracers for myocardial perfusion imaging. Several PET tracers can be used to assess myocardial perfusion.¹⁸ These include ^{82}Rb , ^{13}N - NH_3 , and ^{15}O - H_2O (Figure 4).¹⁹ Both ^{13}N - NH_3 and ^{82}Rb are commonly used for both qualitative and quantitative measurements.^{34,42–44} Visual assessment of PET myocardial perfusion imaging provides high diagnostic accuracy in the detection of CAD.¹⁷ Dynamic imaging analysis permits quantitative assessment of MBF and coronary flow reserve (CFR), which is defined as the

ratio of MBF at peak hyperemia to MBF at rest. CFR measurements provide additional value in the detection of multi-vessel disease and risk stratification of CAD patients.^{45–49} $^{15}\text{O-H}_2\text{O}$ is an ideal myocardial flow tracer to quantify MBF with a linear relation between first-pass extraction and perfusion, but the perfusion images are not of high quality as they are with the other 2 PET tracers (Figure 3).^{19,30,50,51}

^{82}Rb is the most widely used tracer because it is a strontium-82 (^{82}Sr)/ ^{82}Rb generator-produced tracer that does not require a cyclotron for its production.^{52,53} Love et al. initially developed rubidium-86 for myocardial perfusion imaging with a dog.⁷ Following non-human studies, Selwyn et al. applied ^{82}Rb to a human for the first time in 1982.⁵⁴ The short physical half-life of ^{82}Rb (76 seconds) enables sequential rest/stress scanning. ^{82}Rb is a potassium analog, and therefore injected ^{82}Rb is actively transported into myocytes through the Na^+/K^+ adenosine triphosphate (ATP) transport system. This uptake of ^{82}Rb is dependent on MBF and its first-pass retention fraction is approximately 65% at rest. The relatively low lesion contrast with low spatial resolution due to the lower extraction fraction and high positron range is a slight disadvantage of ^{82}Rb .³⁹ In 2000, $^{13}\text{N-NH}_3$ PET was approved by the United States Food and Drug Administration (FDA) to evaluate myocardial perfusion in patients with known or suspected CAD.¹⁹ $^{13}\text{N-NH}_3$ was also approved by the Japanese Ministry of Health and Welfare in March 2012 (Table 2).⁵⁵

The uptake mechanism of $^{13}\text{N-NH}_3$ is unclear. After being taken into the myocyte, $^{13}\text{N-NH}_3$ underwent

metabolic trapping with the conversion of NH_3 to glutamine, glutamic acid, and carbamoyl phosphate.⁵⁶ $^{13}\text{N-NH}_3$ PET is suitable for imaging and measuring of MBF due to its high first-pass extraction fraction and retention in the myocardium with rapid clearance from the blood pool, which also give it high diagnostic accuracy.⁵⁷ The requirement for a cyclotron limits the clinical use of $^{13}\text{N-NH}_3$. Its relatively longer half-life (9.96 minutes) necessitates a longer interval between rest and stress scans, resulting in low throughput in a clinical setting. These are the main disadvantages of $^{13}\text{N-NH}_3$.³⁹ The FDA has approved ^{82}Rb and $^{13}\text{N-NH}_3$ for clinical use (Table 2). The Japanese Ministry of Health, Labour, and Welfare has approved $^{13}\text{N-NH}_3$ for detecting CAD in cases of CAD unable to be diagnosed with using SPECT MPI.⁵⁵

$^{15}\text{O-H}_2\text{O}$ is unique in being metabolically inert and freely diffusible, which are considered ideals for measuring MBF due to the linear relationship between first-pass extraction and perfusion.⁵⁸ The shorter half-life (2.04 minutes) enables consecutive rest/stress protocols, similar to the case with ^{82}Rb .^{59,60} However, $^{15}\text{O-H}_2\text{O}$ requires an on-site cyclotron for tracer production and also is suboptimal for visual assessment due to the low signal-to-noise ratios. These conditions lead to its use being limited in clinical settings. $^{15}\text{O-H}_2\text{O}$ has gained wide popularity in research settings due to its excellent kinetic properties.^{19,61–63} A recent study by Danad et al. examined stress MBF and CFR in 330 patients with CAD,⁶⁴ possibly indicating that $^{15}\text{O-H}_2\text{O}$ could move from research to clinical use.

Fluorine-18 (^{18}F)-flurpiridaz, an analog of the insecticide pyridaben, is a novel MPI tracer that can bind to the mitochondrial complex-1 inhibitor.^{51,65} The positron range of ^{18}F is 1.03 mm, shorter than that of other PET perfusion tracers (Table 2). Injected ^{18}F -flurpiridaz shows very high first-pass extraction and high affinity in myocardial tissue with slow washout from cardiomyocytes (Figure 3). Therefore, accurate quantification of MBF and CFR measurements with high image quality and excellent diagnostic accuracy are expected.^{66–68} Because of the longer half-life of ^{18}F (109.8 minutes), delivery of unit doses from regional cyclotrons may be possible, similar to the case with fluorine-18-labeled fluorodeoxyglucose (^{18}F -FDG). In the meantime, repeated measurements of stress and rest studies would likely be difficult due to the longer half-life, and therefore a separate day protocol or some correction for the residual activity of the first acquisition might be needed. Phase 2 clinical trials showed promise,⁶⁷ and phase 3 clinical trials demonstrated the diagnostic usefulness for specific subpopulations such as women and obese patients.

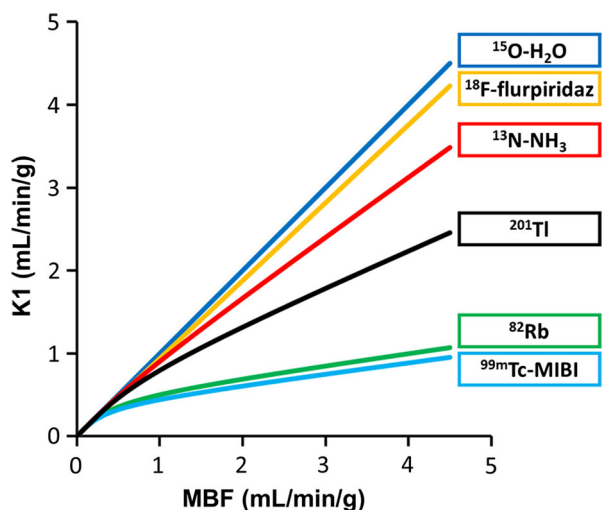


Figure 3. Extraction fraction of each perfusion tracer The extraction fraction of $^{15}\text{O-H}_2\text{O}$ is nearly 100% due to its exclusive property of being metabolically inert and freely diffusible. The extraction fraction of ^{82}Rb is lower than that of the other PET tracers. ^{201}Tl has a higher extraction fraction compared to that associated with $^{99\text{m}}\text{Tc-MIBI}$.

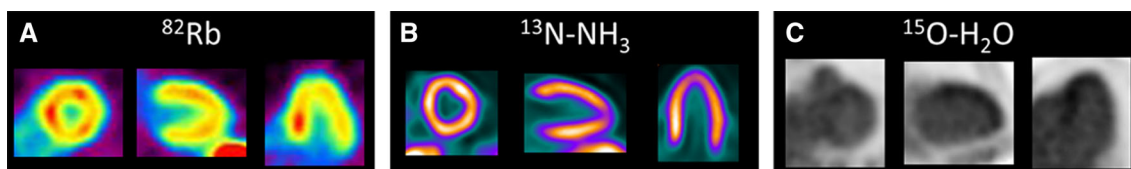


Figure 4. Qualitative images of PET tracers ^{82}Rb PET has relatively low lesion contrast with low spatial resolution. $^{13}\text{N-NH}_3$ PET shows clear images due to rapid clearance from the blood pool. With $^{15}\text{O-H}_2\text{O}$ PET, it is difficult to distinguish between myocardium and blood pool.

Metabolic Imaging

The heart derives its energy from a variety of sources such as free fatty acids (FFA), glucose, lactate, and ketone bodies (Figure 5).⁶⁹ Glucose metabolism dominates after feeding, and fatty-acid metabolism dominates under long-fasting conditions.⁶⁹ Carbohydrates taken into cardiomyocytes are metabolized into pyruvic acid using various enzymatic actions. If oxygen supply is sufficient, ATPs are produced from glucose via the glycolysis system in the tricarboxylic acid (TCA) cycle and electron transfer system.⁷⁰ In the ischemic state, acid metabolism is impaired due to insufficient oxygen supply to the myocardium.⁷¹ Alternatively ATP is produced from lactic acid because anaerobic glycolysis with less oxygen consumption becomes predominant. However, anaerobic glycolysis produces less ATP than does aerobic glycolysis. If severe myocardial ischemia continues, myocardial cells become necrotic as ATP production diminishes.⁷² Several SPECT and PET tracers have been used or tried clinically to assess myocardial metabolism (Table 3, Figure 6).

SPECT tracers for metabolic imaging. For fatty acid metabolism evaluation, SPECT examination using iodine-123-labeled beta-methyl-*p*-iodophenylpentadecanoic acid ($^{123}\text{I-BMIPP}$) has been clinically used in Japan.^{44,73,74} However, $^{123}\text{I-BMIPP}$ was initially developed in the United States and the first human use was in 1986 by Knapp et al.⁷⁵ After the initial development in the US, the Japanese community took over development of $^{123}\text{I-BMIPP}$. The first human use in Japan was reported in 1991 in a Japanese article.⁷⁶ Following this Japanese article, Kurata et al. reported Japanese $^{123}\text{I-BMIPP}$ data in an international journal in 1992.⁷⁷ $^{123}\text{I-BMIPP}$ is an iodinated fatty-acid analog used to assess myocardial fatty acid metabolism.^{78,79} This tracer, however, is not approved for clinical use in the US despite its successful for clinical use even successive early experience use in that country.⁸⁰ Iodine-123-labeled iodophenylpentadecanoic acid ($^{123}\text{I-IPPA}$) is a radiolabeled free fatty acid (FFA) analog which is in phase 3 trials in United States but which has not yet been approved.⁸¹

Following intravenous injection, $^{123}\text{I-BMIPP}$ and $^{123}\text{I-IPPA}$ are rapidly distributed to various organs, such as liver and heart, and cleared rapidly from the blood.^{81–84} Initial uptake of the administered dose of $^{123}\text{I-BMIPP}$ is assumed to be about 6% by the heart and 14% by the liver. The residual $^{123}\text{I-BMIPP}$ is distributed uniformly in other organs and tissues.^{76,85,86} After initial uptake, only a portion of the $^{123}\text{I-BMIPP}$ and $^{123}\text{I-IPPA}$ is metabolized immediately to water-soluble low-molecular-weight products. Most of the $^{123}\text{I-IPPA}$ undergoes metabolism similar to that of long-chain fatty acids, through rapid mitochondrial beta-oxidation.^{87,88} The initial and late clearance of $^{123}\text{I-IPPA}$ are thought to reflect β -oxidation and clearance of tracer incorporated into triglyceride pools, respectively.⁸⁸ $^{123}\text{I-IPPA}$ images show minimal background activity and good image quality. The metabolism of $^{123}\text{I-BMIPP}$ is slower than that of $^{123}\text{I-IPPA}$ because $^{123}\text{I-BMIPP}$ is a modified-branched fatty acid analog with a methyl group on the beta-carbon. Both of the end products are excreted in a conjugated form in the urine.^{76,89,90}

$^{123}\text{I-BMIPP}$ scintigraphy when combined with perfusion imaging may show preserved perfusion, but fatty acid metabolism is impaired as myocardium shifts from metabolizing fatty acids to metabolizing predominantly glucose following ischemic episodes. Therefore, the region of perfusion-metabolic mismatch ($^{123}\text{I-BMIPP}$ defect larger than perfusion defect) indicates the presence of ischemic myocardium (Figure 7).^{80,91–93} $^{123}\text{I-BMIPP}$ has been approved in Japan only for clinical use.⁴⁴

PET tracers for metabolic imaging. $^{18}\text{F-FDG}$ is the most frequently used tracer around the world and is employed mainly for the assessment of malignant tumors. For the purposes of nuclear cardiology imaging, $^{18}\text{F-FDG}$ PET was first used to define and identify viable myocardium in CAD in the 1980 s.⁹⁴ Since $^{18}\text{F-FDG}$ is an analog of glucose, once taken up into the cardiomyocytes via the glucose transporter (GLUT), it is phosphorylated to $^{18}\text{F-FDG-6-phosphate}$ by hexokinase as well as glucose.⁹⁵ $^{18}\text{F-FDG-6-phosphate}$ accumulates intracellularly without being metabolized during glycolysis, a condition referred to as “metabolic trapping” (Figure 6). Therefore, myocardial viability can be

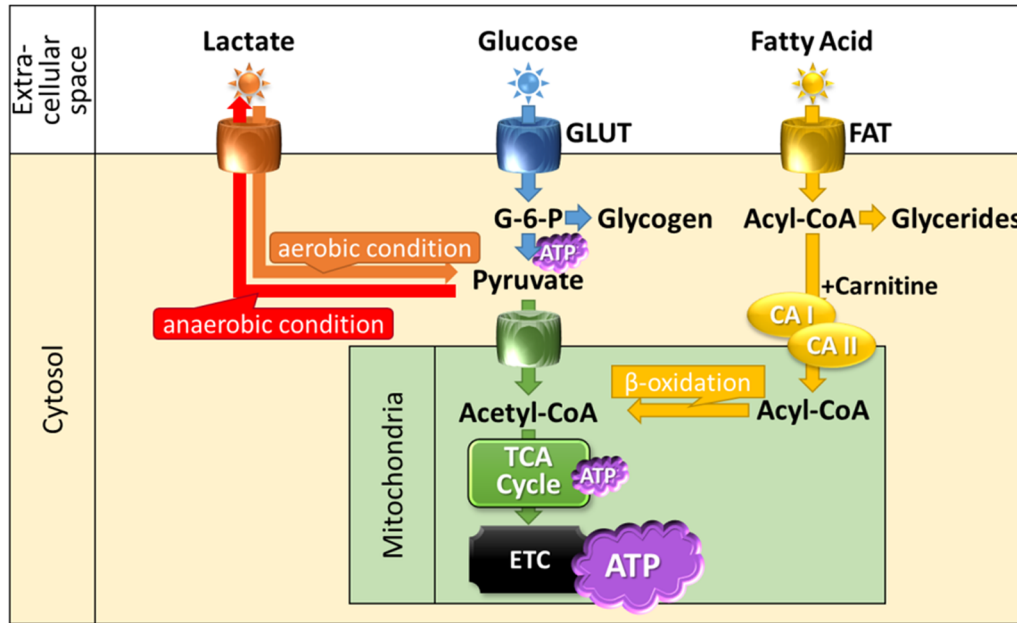


Figure 5. Schematic representation of cardiac energy metabolism. Substrates are transported across the extracellular membrane into the cytosol through GLUT for glucose and FAT for fatty acid. Metabolized intermediates such as pyruvate and acyl-CoA are transported across the inner mitochondrial membrane for oxidation. Then inside the mitochondrion, substrates are oxidized or carboxylated and fed into the TCA cycle and ETC to produce ATP. GLUT, glucose transporter; FAT, fatty acid transporter; G-6-P, glucose-6-phosphate; ATP, adenosine triphosphate; TCA, tricarboxylic acid; ETC, electron transport chain; CA I, carnitine acyltransferase I; CA II, carnitine acyltransferase II.

evaluated by assessing the accumulation of ^{18}F -FDG in myocardium. To determine myocardial viability, oral glucose loading or an insulin-glucose clamp is applied to enhance ^{18}F -FDG uptake in viable myocardium.^{96,97} In ischemic myocardium, ^{18}F -FDG accumulation in the myocardium is maintained under a fasting condition due to the dominant anaerobic glucose metabolism. On the other hand, in the infarcted scar tissue, ^{18}F -FDG accumulation is absent due to non-availability of glucose metabolism. In a clinical setting, ^{18}F -FDG PET viability assessment is performed using the myocardial perfusion image obtained by SPECT or PET.^{94,98} A region with preserved ^{18}F -FDG accumulation but reduced myocardial perfusion indicates viable myocardium. In such a case, functional recovery after coronary revascularization is likely especially with extensive mismatch pattern.

^{11}C -palmitate and fluorine-18-labeled fluoro-6-thiaheptadecanoic acid (^{18}F -FTHA) have been used to evaluate fatty acid metabolism.^{99–101} Similar to the case with ^{18}F -FDG PET, a shift in myocardial metabolism from fatty acid to glucose can be estimated using these fatty acid analogs.¹⁰²

Myocardial oxygen metabolism can be non-invasively evaluated by ^{11}C -acetate PET.^{103,104} ^{11}C -acetate

taken into myocardium is converted into acetyl-CoA, consecutively metabolized and excreted into ^{11}C -CO₂ via the TCA cycle. The ^{11}C -acetate clearance rate is used to assess myocardial oxygen consumption since TCA cycle activity is directly linked with myocardial oxygen consumption which is independent of the concentration of energy substrates for the myocardium.^{105,106} ^{11}C -acetate PET allows for non-invasive observation of regional myocardial oxygen metabolism in the presence of ischemia,^{107,108} cardiomyopathy,^{109,110} and heart failure (HF) in a state of deprived energy.^{111,112} Myocardial oxidative metabolism in the RV can also be estimated using ^{11}C -acetate PET.^{113–116} ^{11}C -acetate PET permits the evaluation of both blood flow and oxygen metabolism with one examination using some model analysis due to the relatively high extraction fraction.⁶²

Sympathetic Imaging

The heart has extensive innervation, both sympathetic and parasympathetic. The sympathetic nervous system uses norepinephrine (NE), and the parasympathetic nervous system uses acetylcholine (Ach) as the main neurotransmitters. NE is synthesized from the

Table 3. Tracers for metabolic imaging

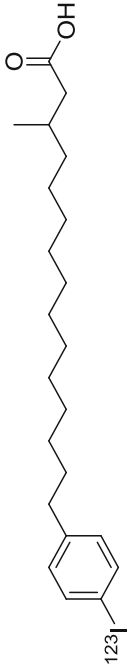
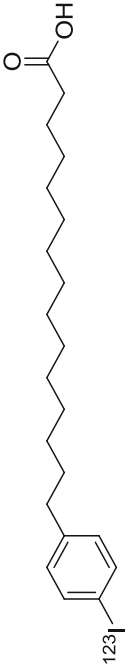
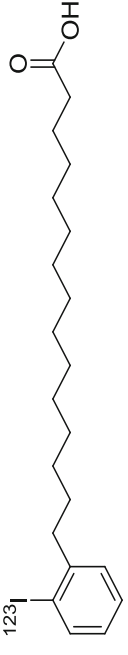
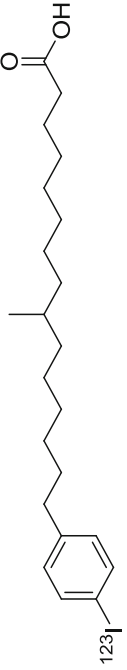
Tracer	Chemical structure	Characteristics	Approval year	
			FDA	Europe Japan
SPECT ^{123}I -BMIPP		Long-chain fatty acid analogue	-	1993
^{123}I <i>p</i> -IPPA		Long-chain fatty acid analogue	-	-
^{123}I <i>o</i> -IPPA		Long-chain fatty acid analogue	-	-
^{123}I -9-MPA		Long-chain fatty acid analogue	-	-

Table 3 continued

Tracer	Chemical structure	Characteristics	Approval year		
			FDA	Europe	Japan
PET ¹⁸ F-FDG		Glucose analog	1997	1994*	2002
¹⁸ F-FTHA		Long-chain fatty acid analog	-	-	-
¹¹ C-palmitic acid		Long-chain fatty acid analog	-	-	-
¹¹ C-acetic acid		¹¹ C labeled acetic acid, oxidative metabolism	-	-	-

BMIPP, beta-methyl-p-iodophenylpentadecanoic acid; *IPPA*, iodophenylpentadecanoic acid; *9-MPA*, iodophenyl-9-methyl-pentadecanoic acid; *FDG*, fluorodeoxyglucose; *FTHA*, fluoro-6-thia-heptadecanoic acid
 *EURD List Juli 2017: http://www.ema.europa.eu/docs/en_GB/document_library/Other/2012/10/WC500133159.xls

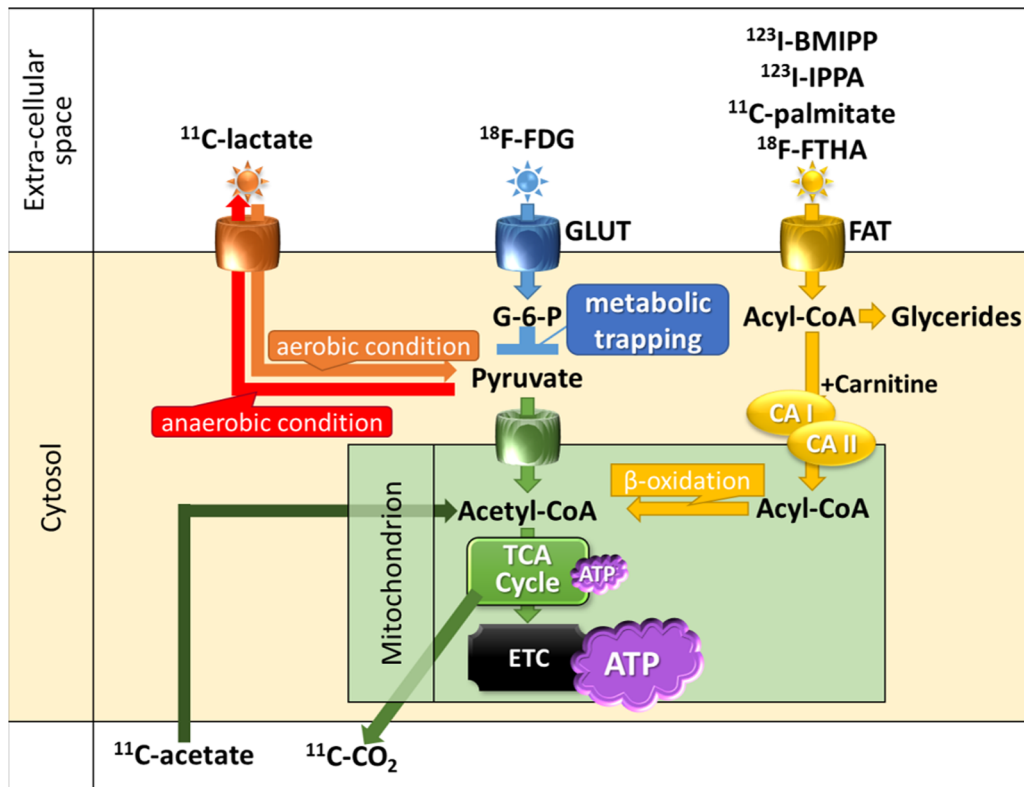


Figure 6. Tracers for assessing cardiac energy metabolism ^{18}F -FDG is a glucose analog in which the oxygen in position C-2 is replaced with ^{18}F . ^{18}F -FDG is actively transported into the cell mediated by GLUT in the same way as glucose. Once inside the cell, glucose and ^{18}F -FDG are phosphorylated by hexokinase. Phosphorylated glucose (G-6-P) continues along the glycolytic pathway for energy production. However, ^{18}F -FDG-6-phosphate cannot enter glycolysis and is trapped intracellularly in a condition known as “metabolic trapping.” GLUT, glucose transporter; G-6-P, glucose-6-phosphate; FDG, ^{18}F -fluorodeoxyglucose; FDG-6-P, ^{18}F -FDG-6-phosphate.

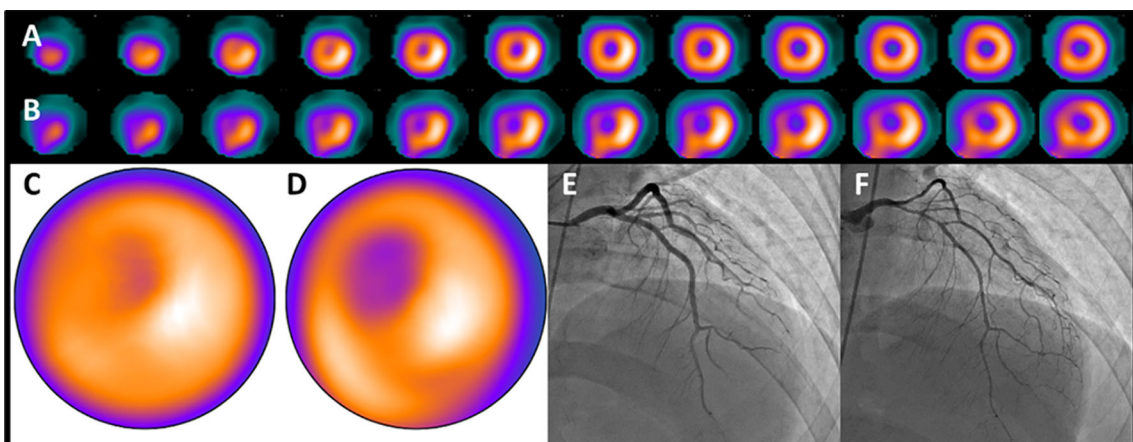
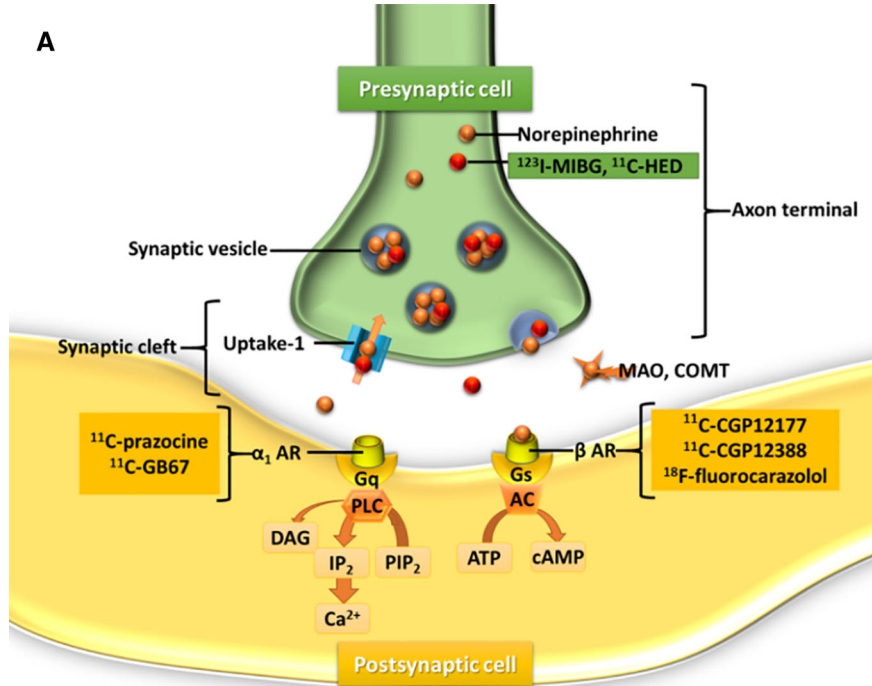
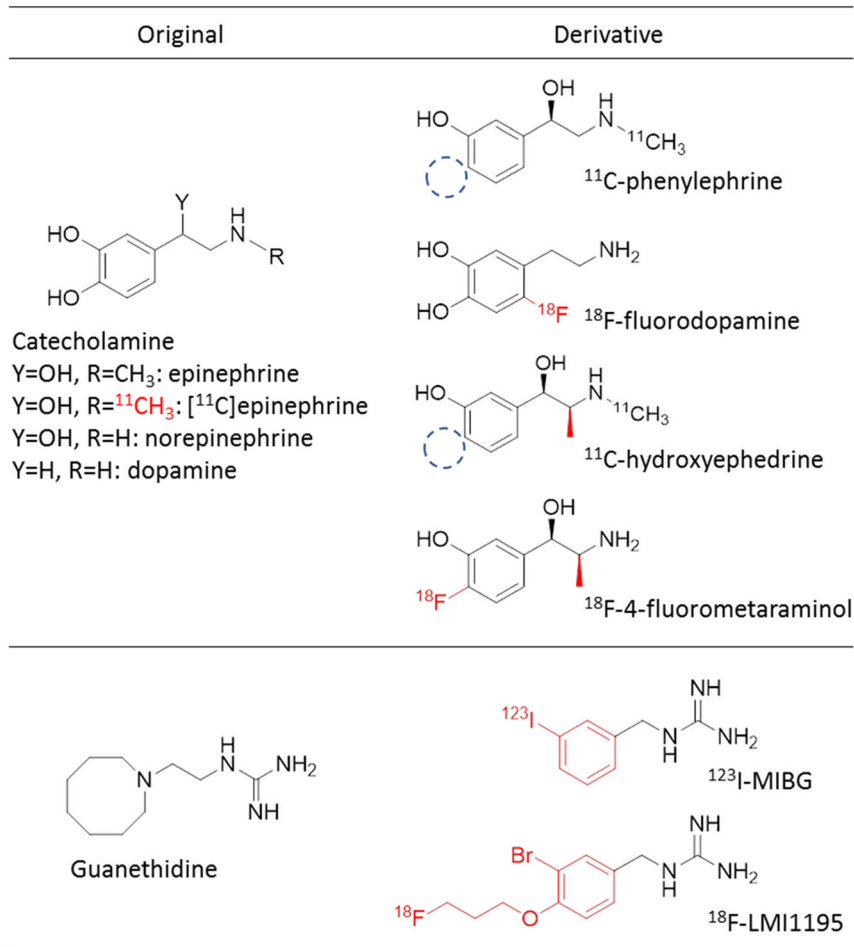


Figure 7. Ischemic memory imaging Perfusion image of $^{99\text{m}}\text{Tc}$ product shows slightly reduced perfusion (A, C), whereas moderately reduced ^{123}I -BMIPP uptake is seen in the anterior to septal wall (B, D), which indicates perfusion-metabolic mismatch. Coronary angiogram shows no significant stenosis (E); however, vasospastic angina in the left anterior descending artery due to the spasm is proved through intracoronary injection of acetylcholine (F).



B



◀**Figure 8.** Schema of myocardial adrenergic neuronal terminals. Figure A shows the schematic representation of myocardial adrenergic neuronal terminals and Figure B shows the chemical structure of each tracer. MIBG is actively taken up into sympathetic nerves through the uptake-1 mechanism and then stored in the synaptic vesicle in a manner similar to that for norepinephrine (NE). Nerve stimulation releases MIBG and NE into the synaptic cleft through exocytosis. MIBG does not bind to the postsynaptic receptor and is not metabolized by monoamine oxidase (MAO) or catechol-O-methyltransferase (COMT). Most of the released MIBG undergoes reuptake through the uptake-1 mechanism, and the remaining MIBG goes into the blood (spillover). ¹²³I-MIBG, *m*-[¹²³I]iodobenzylguanidine; ¹¹C-HED, ¹¹C-hydroxyephedrine; DAG, diacylglycerol; AR, adrenergic receptor; Gq, phospholipase C-coupled Gq-protein; Gs, phospholipase C-coupled Gs-protein; ATP, adenosine triphosphate; cAMP, cyclic adenosine monophosphate; IP₂, inositol bisphosphate; PIP₂, phosphatidylinositol biphosphate.

amino acid tyrosine in presynaptic neurons (Figure 8). NE is transported into the presynaptic neuronal terminal vesicles by the vesicular monoamine transporter (VMAT). Exocytosis is led by the activation of voltage-dependent calcium channels and vesicles at the presynaptic neuron. Some of the NE released into the synaptic cleft binds to the adreno-receptors for downstream effects, while much of the NE undergoes reuptake into presynaptic neurons via the terminal transporter (uptake-1).^{117–119}

The sympathetic nerve is vulnerable to ischemia, and sympathetic nervous function may decline even if myocardial blood flow at rest is maintained.¹²⁰ In HF, continued stimulation of the β₁ receptor due to increased norepinephrine levels results in a decrease of receptor density (down regulation), with corresponding poor reactivity to the stimulation. Moreover, in a persistent state of sympathetic hyperactivity, the ability to retain norepinephrine is also decreased at the nerve terminal end.¹²¹ Abnormal neuro-hormonal function is reported in various heart diseases, and worsening of neuronal function is associated with cardiac events and sudden cardiac death.^{122–124}

SPECT tracers for sympathetic imaging. Iodine-123-labeled metaiodobenzylguanidine (¹²³I-MIBG) is widely used as a SPECT tracer to evaluate the presynaptic sympathetic innervation of the heart.^{125–127} The first use of ¹²³I-MIBG in humans was in 1981 by a University of Michigan group.¹²⁸ It is an analog of catecholamine, which is taken up via the uptake-1 mechanism and stored in synaptic vesicles as is NE. Tracers are released into the synaptic cleft from the synaptic vesicle via the exocytosis pathway, but do not lead to any physiological activity without binding to the catecholamine receptor. Since it is not metabolized by

monoamine oxidase (MAO) or catechol-O-methyltransferase (COMT), most of the released tracer is reabsorbed at the synapse terminal and again stored in synaptic vesicles. Therefore, information reflecting the process of ¹²³I-MIBG uptake into the synapse terminal, storage in the vesicles, secretion, reabsorption, and release into the blood is obtained from sympathetic imaging.^{129,130} An early anterior planar image at 15 minutes after injection and a late anterior planar image starting at 3 to 4 hours after injection are acquired to calculate the heart-to-mediastinum ratio (HMR) and the washout ratio (Figure 9). These parameters are considered to be standards. The high liver uptake and relatively high energy of the tracers make the image quality suboptimal. It is difficult to evaluate SPECT images especially in severe HF, which usually has limited myocardial ¹²³I-MIBG radioactivity. Therefore, planar data acquisition is standard for ¹²³I-MIBG imaging.¹³¹ Although these images present an easily obtained index, inter-institutional differences of the HMR due to differences in camera-collimator systems being used have hampered multicenter comparisons. Recently, standardization among different collimator types has been achieved using the calibration phantom and could easily be extrapolated to the images of other institutions.^{132,133} Late HMR provides the relative distribution of cardiac sympathetic nerve terminals, which is related to neuronal function from uptake to release. Washout ratio represents the information of the sympathetic drive. Several studies have presented that patients with chronic HF and a low late HMR and/or an increased washout rate are at increased risk for cardiac death.

PET tracers for sympathetic imaging. As a PET tracer, carbon-11-labeled hydroxyephedrine (¹¹C-HED) is used mainly to assess presynaptic cardiac sympathetic nerve distribution.¹³⁴ ¹¹C-HED is still the most widely used PET tracer for sympathetic nervous function imaging in mainly research settings.¹³⁵ Extracardiac uptake is mainly by the liver with very limited lung uptake. In ischemic heart disease, a mismatch region of myocardial blood flow and sympathetic dysfunction is reported as a decision criterion for prediction of fatal arrhythmia and indication for cardioverter-defibrillator implantation (ICD).^{136,137} The distribution abnormality of cardiac sympathetic denervation has been demonstrated in previous ¹¹C-HED studies, including those involving patients with HF,^{138,139} cardiac arrhythmias,^{140,141} myocardial infarction,^{142,143} cardiac diabetic neuropathy,^{144,145} and HF with preserved ejection fraction (HFpEF).¹⁴⁶

N-[3-bromo-4-(3-¹⁸F-fluoro-propoxy)-benzyl]-guanidine (LMI 1195) is a novel ¹⁸F-labeled ligand to image the norepinephrine transporter.¹⁴⁷ ¹⁸F-fluorometaraminol,¹⁴⁸ ¹¹C-phenylephrine,¹⁴⁹ ¹⁸F-fluorodopamine,¹⁵⁰ and

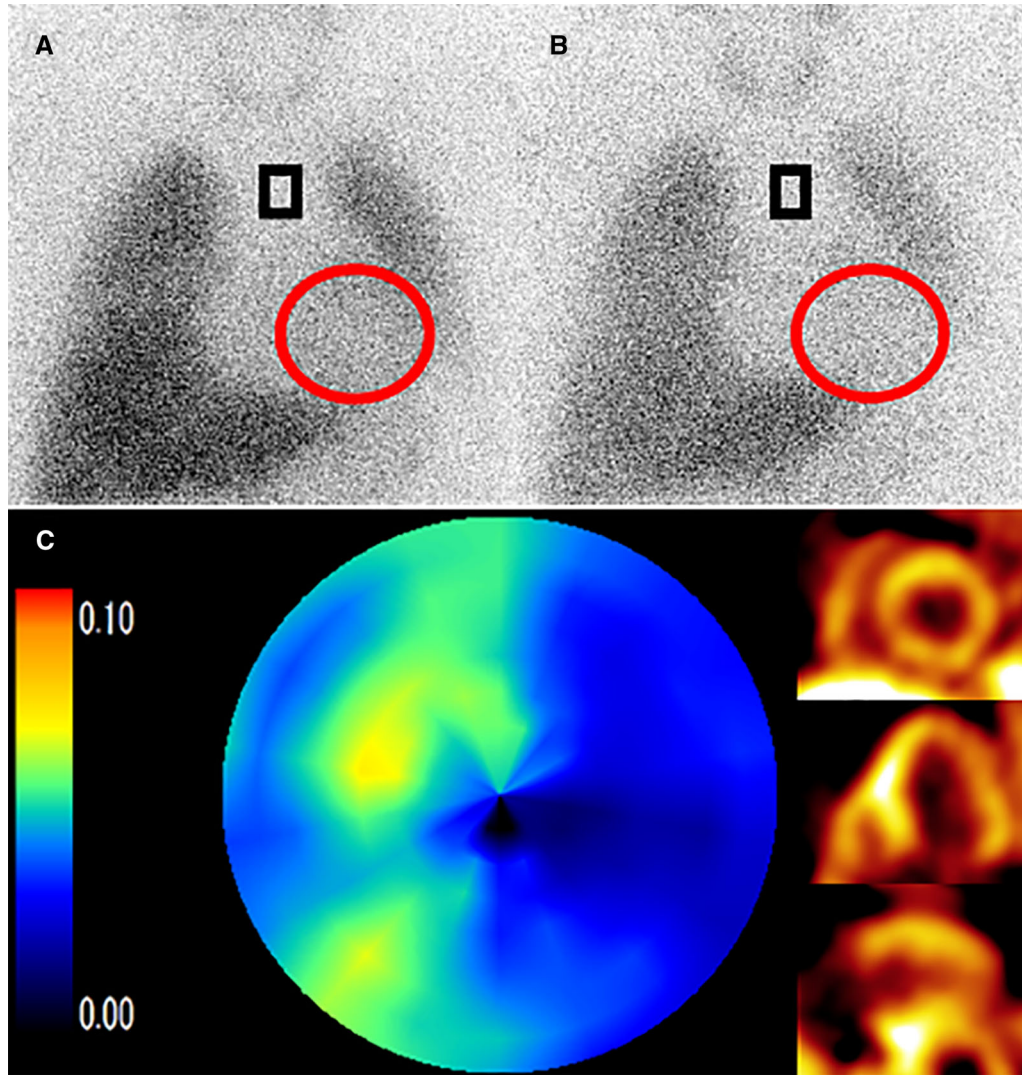


Figure 9. Representative case of ^{123}I -MIBG scintigraphy and ^{11}C -hydroxyephedrine PET. A male in his 40s suffered from dilated cardiomyopathy, with a left ventricular ejection fraction of approximately 30%. An early anterior planar image at 15 min after injection (A) and a late anterior planar image starting at 4 hours after injection (B) are acquired to calculate the heart-to-mediastinum ratio (HMR) and the washout ratio. Calculated early HMR, delayed HMR, and washout ratio were 1.7, 1.4, and 40.3%, respectively. Whole retention index from ^{11}C -hydroxyephedrine PET was calculated as 0.044. Distribution of sympathetic nerve system was lower especially in the lateral wall.

^{11}C -epinephrine¹⁵¹ are the other radiotracers for evaluating presynaptic neuronal function. Several tracers such as ^{18}F -fluorocarazolol,¹⁵² 4-[3-[(1,1-dimethylamino)-2-hydroxypropoxy]-1,3-dihydro-2H-benzimidazol-2- ^{11}C -one (^{11}C -CGP12177),¹⁵³ and (S)-4-(3-(2'- ^{11}C -isopropylamino)-2-hydroxypropoxy)-2H-benzimidazol-2-one (^{11}C -CGP 12388)¹⁵⁴ have been reported for assessing postsynaptic sympathetic neuronal functions through measurement of myocardial β -adrenergic receptor (β -AR) density, which directly regulates LV systolic function.¹⁵⁵ There are several

reports regarding tracers for imaging the parasympathetic nervous system,^{156,157} but the clinical role of these has not yet been established (Table 4).

Imaging of Inflammation and Atherosclerosis

Nuclear medicine imaging can be used to view several in vivo pathological processes in inflammation and atherosclerosis. Several novel tracers may have uses

Table 4. Tracers for sympathetic imaging

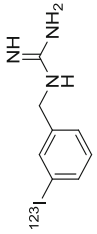
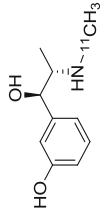
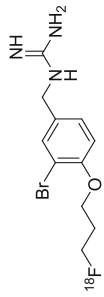
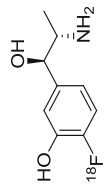
	Tracer	Chemical structure	Approval year	
			FDA	Europe Japan
Sympathetic nervous system Presynaptic Catecholamine derivative	^{123}I -MIBG		2008	1995* * 1992
	^{11}C -hydroxyephedrine		-	-
	^{18}F -LMI1195		-	-
	^{18}F -4-fluorometaraminol (4-[^{18}F]fluorometaraminol)		-	-

Table 4 continued

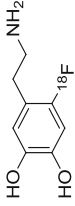
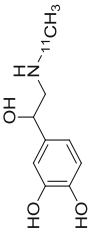
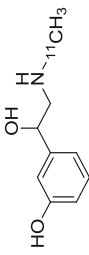
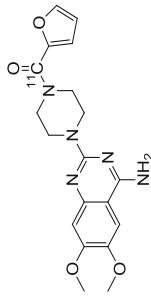
Tracer	Chemical structure	Approval year		
		FDA	Europe	Japan
Catecholamine		-	-	-
		-	-	-
		-	-	-
Postsynaptic α ₁ -receptor		-	-	-

Table 4 continued

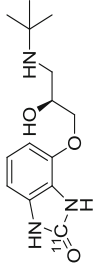
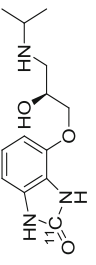
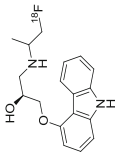
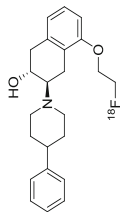
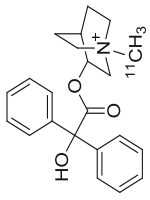
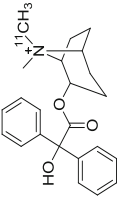
	Tracer	Chemical structure	Approval year		
			FDA	Europe	Japan
β-receptor	¹¹ C-CGP12177		-	-	-
	¹¹ C-CGP12388		-	-	-
	¹⁸ F-fluorocarazolol		-	-	-
Parasympathetic nervous system					
Presynaptic	Vesicular acetylcholine transporter	¹⁸ F-fluoroethoxybenzovesamicol	-	-	-
					

Table 4 continued

	Tracer	Chemical structure	Approval year		
			FDA	Europe	Japan
Postsynaptic	Muscarine		-	-	-
	¹¹ C-methyl QNB				
			-	-	-
	¹¹ C-methyl TRB				

** EURD list nov 2012 http://www.ema.europa.eu/docs/en_GB/document_library/Other/2012/04/WC500124999.xls

Table 5. Inflammation and atherosclerosis imaging

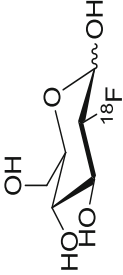
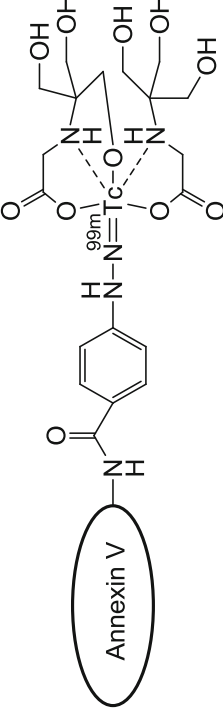
Isotope	Radiopharmaceutical	Type of tracer	Study population	Characteristics	Approval year		
					FDA	Europe	Japan
General inflammation ^{18}F	^{18}F -FDG 	Organic compound	Carotid and coronary plaque imaging Cardiac sarcoidosis Device infection	Accumulating macrophage Strong signal Limitation: non-specific myocardial accumulation	-	1994*	2012 (cardiac sarcoidosis)
^{67}Ga	$^{67}\text{Ga}^{3+}$	Metal cation	Inflammatory heart disease Cardiac sarcoidosis	No physiological uptake Limitation: suboptimal image quality	1976	1972*	1982
Infection ^{111}In	^{111}In WBC	Radiolabeled cell	Infectious disease	Accumulates in WBC Limitation: suboptimal image quality	1985	1980**	1992
Atherosclerosis imaging $^{99\text{m}}\text{Tc}$	$^{99\text{m}}\text{Tc}$ annexin 5 	Radiometal-tagged Annexin V	Apoptosis imaging	Lesion specific Limitation: weak signal intensity	-	-	-

Table 5. continued

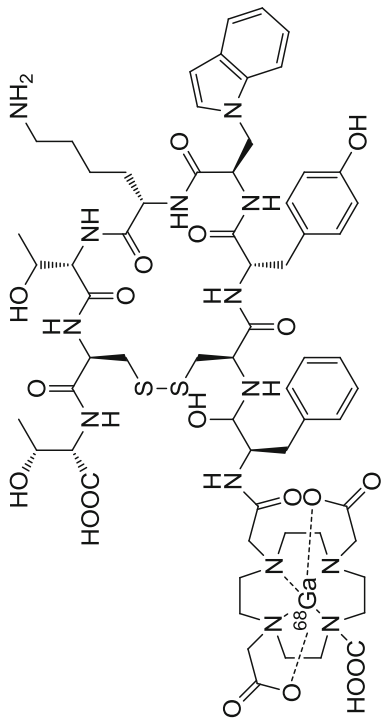
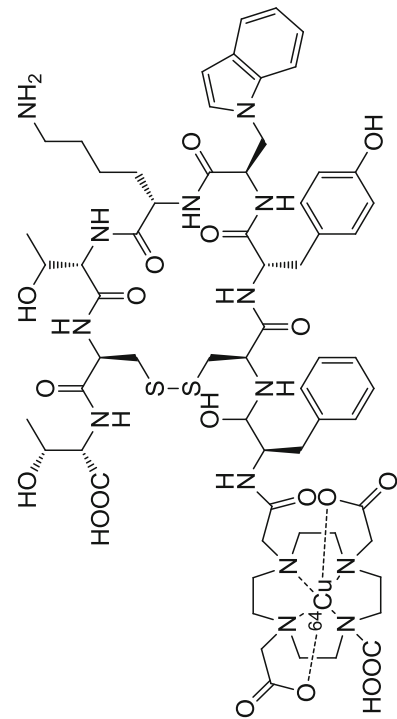
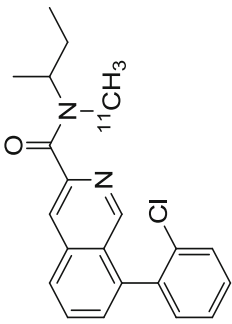
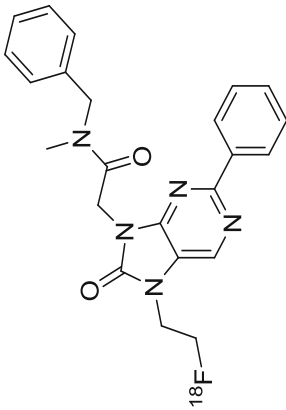
Isotope	Radiopharmaceutical	Type of tracer	Study population	Characteristics	Approval year		
					FDA	Europe	Japan
⁶⁸ Ga	⁶⁸ Ga DOTATATE	Radiometal-tagged octreotide analog	Symptomatic carotid atherosclerosis Unstable angina	Accumulates activated macrophages No physiological myocardial uptake Generator produced	2016	-	-
							
⁶⁴ Cu	⁶⁴ Cu DOTATATE	Radiometal-tagged octreotide analog	Symptomatic carotid atherosclerosis	Good image quality	-	-	-
							

Table 5. continued

Isotope	Radiopharmaceutical	Type of tracer	Study population	Characteristics	Approval year		
					FDA	Europe	Japan
^{11}C	Translocator protein ^{11}C -PK11195	Organic compound 	Symptomatic carotid atherosclerosis	Accumulates in activated mononuclear phagocyte	-	-	-
^{18}F	^{18}F -FEDAC	Organic compound 		Accumulates in activated mononuclear phagocyte High affinity and better image quality	-	-	-
^{18}F	^{18}F -NaF	Inorganic anion	Aortic stenosis Coronary artery disease Carotid artery plaque	Accumulates in calcification lesion	2012	-	-

^{68}Ga DOTATATE, Gallium-68-labeled [1,4,7,10-tetraazacyclododecane-N,N',N''-tetraacetic acid]-d-Phe¹, Tyr³-octreotate; ^{18}F -FDG, ^{18}F -fluorodeoxyglucose; ^{18}F -FEDAC, N-benzyl-N-methyl-2-[7,8-dihydro-7-(2-[^{18}F]fluoroethyl)-8-oxo-2-phenyl-9H-purin-9-yl]acetamide; WBC, white blood cell
* EURD List July 2017: http://www.ema.europa.eu/docs/en_GB/document_library/Other/2012/10/WC500133159.xls
** EURD list 2012 http://www.ema.europa.eu/docs/en_GB/document_library/Other/2012/04/WC500124999.xls

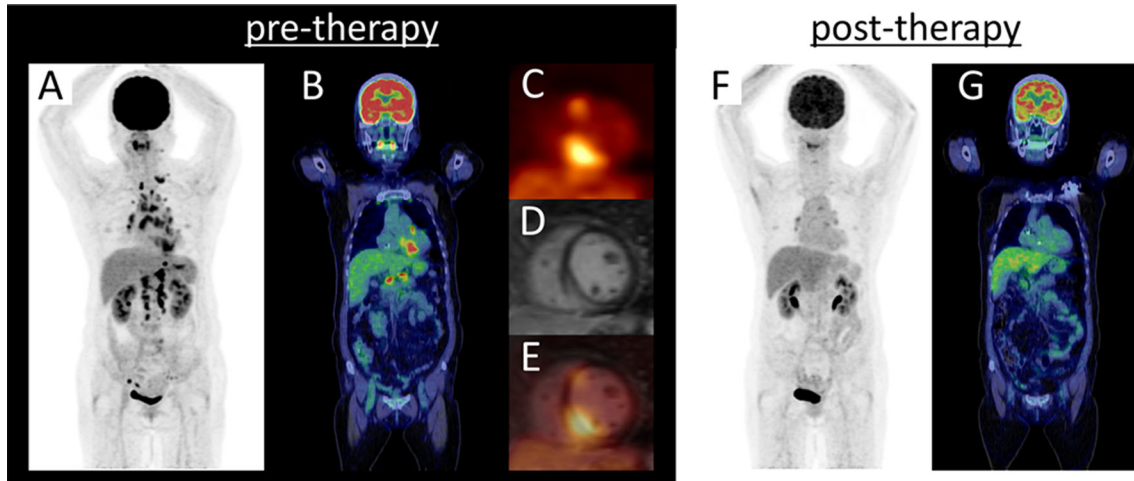


Figure 10. Representative case of cardiac sarcoidosis. Maximum intensity projection (MIP) image of ^{18}F -FDG PET (A), PET/CT coronal image (B), short-axis image of ^{18}F -FDG PET (C), late gadolinium enhancement (LGE)-MRI (D), and fused image of ^{18}F -FDG PET and LGE-MRI (E) at pre-therapy, MIP image of ^{18}F -FDG PET (F) and PET/CT coronal image (G) at post-therapy (steroid 30 mg/1 month) are displayed. ^{18}F -FDG PET detected focal cardiac uptake and multiple lymph node disease in the supraclavicular, mediastinum, hilum, abdominal, and pelvis region at pre-therapy. ^{18}F -FDG uptake is seen at the same site of LGE-MRI abnormal intensity. At post-therapy, ^{18}F -FDG uptakes were markedly lower. ^{18}F -FDG is useful not only for diagnosis but also to confirm the effectiveness of treatments.

for tracking inflammation, hypoxia, or active calcification (Table 5).

SPECT tracers for imaging of inflammation and atherosclerosis. Gallium-67 (^{67}Ga) scintigraphy has been used to detect inflammatory lesions including infection and sarcoidosis.^{158,159} Several factors influence ^{67}Ga accumulation in inflammatory lesions. These factors include increased delivery and accumulation of transferrin-bound ^{67}Ga due to increased blood flow and vascular membrane permeability. The tendency of ^{67}Ga to bind to lactoferrin and leukocytes also leads to highly concentrated uptake of ^{67}Ga .¹⁶⁰ Imaging is performed at 48 to 72 hours after tracer injection. In clinical settings, physicians ideally look to have results immediately following a diagnostic test, and therefore a late imaging protocol is one of the major limitations of ^{67}Ga . ^{67}Ga scanning is useful to differentiate acute myocarditis from acute myocardial infarction.¹⁶¹ ^{67}Ga scintigraphy has been a major analytical tool in the diagnosis of cardiac sarcoidosis.¹⁶² There is no significant distribution in normal myocardium.¹⁶³ This is an advantage of ^{67}Ga when applied to cardiac sarcoidosis. However, generally speaking, ^{67}Ga has a limited role in the evaluation and management of sarcoidosis.¹⁶³

Inflammatory cells such as granulocytes, lymphocytes, and macrophages are migrated into inflammatory

lesions, resulting in the activation of a biological defense mechanism. SPECT imaging with indium-111 (^{111}In)-radiolabeled autologous white blood cells (WBC) has proven to be valuable in the detection of endocarditis. ^{111}In -WBC is highly specific for infectious lesions because granulocytes are recruited to the site of inflammatory foci but have limited sensitivity due to a weak signal.^{164–166}

Apoptosis imaging. Tissue apoptosis is considered to be one of the earlier stages of vascular plaque rupture,¹⁶⁷ and therefore detecting apoptotic lesions may precipitate effective treatments to prevent cardiovascular events. Apoptotic cells externalize negatively charged phosphatidylserine (PS).¹⁵ Human protein annexin A5 binds to PS. $^{99\text{m}}\text{Tc}$ -labeled annexin A5 has been shown to have higher uptake in the carotid arteries of vulnerable stroke patients.¹⁶⁸ $^{99\text{m}}\text{Tc}$ -tagged annexin A5 specifically accumulates in vascular atherosclerotic lesions, which is a great advantage. In contrast, the signal intensity of $^{99\text{m}}\text{Tc}$ -labeled annexin A5 is quite a bit lower than that of ^{18}F -FDG.¹⁶⁹ $^{99\text{m}}\text{Tc}$ -labeled annexin A5 drew much interest a decade ago but has not had wide clinical application, perhaps due to the lower signal intensity and tracer availability.

PET tracers for imaging of inflammation and atherosclerosis. Glucose is consumed in large quantities in the inflammatory process, and therefore

active inflammatory lesions show high ^{18}F -FDG accumulations. It is necessary to suppress physiological myocardial glucose metabolism in order to accurately evaluate myocardial inflammatory lesions using ^{18}F -FDG PET. Among effective approaches to reducing physiological myocardial glucose metabolism, long-period fasting is the most common. Long-period fasting combined with a low-carbohydrate diet and/or high-fat diet and unfractionated heparin intravenous injection are also used. These approaches lead to myocardial free fatty acid metabolism dominance.¹⁷⁰ ^{18}F -FDG PET is more useful than are perfusion SPECT and delayed enhanced cardiac magnetic resonance (CMR) to not only diagnose but also monitor treatment effects in inflammatory heart disease such as cardiac sarcoidosis (Figure 10).¹⁷¹ Myocardial ischemia (reflecting a shift to glucose metabolism), other cardiomyopathy (reflecting microcirculatory ischemia and inflammation), and cardiac tumors also show ^{18}F -FDG accumulation.^{172–175}

Incomplete suppression of physiological myocardial ^{18}F -FDG uptake may cause false positives. Therefore, new tracers have been developed to detect inflammatory heart disease and atherosclerotic lesions. These radiopharmaceuticals target tissue apoptosis, tissue calcification, activated macrophages, and tissue hypoxia.

^{68}Ga complexed with [1,4,7,10-tetraazacyclododecane-1,4,7,10-tetraacetic acid]-1-Na³-octreotide (^{68}Ga -DOTANOC),¹⁷⁶ fluorine-18 fluorothymidine (^{18}F -FLT),¹⁷⁷ ^{68}Ga complexed with [1,4,7,10-tetraazacyclododecane-1,4,7,10-tetraacetic acid]-Phe¹-Tyr³-octreotide (^{68}Ga -DOTATOC),¹⁷⁸ and fluorine-18 fluoromisonidazole (^{18}F -FMISO)¹⁷⁹ have been reported to improve specificity with regard to diagnosis of cardiac sarcoidosis.

^{68}Ga -tagged tracers can be prepared using a generator system and have been applied for clinical oncology imaging. Activated macrophages show upregulated G-protein-coupled somatostatin receptor subtype-2 receptors. In an observational study involving oncology patients, uptake of ^{68}Ga complexed with a somatostatin analog, 1,4,7,10-tetraazacyclododecane-1,4,7,10-tetraacetic acid-D-Phe¹-Tyr³-octreotate (^{68}Ga -DOTATATE), in large arteries increased in relation to age.¹⁸⁰ A recent study prospectively revealed ^{68}Ga -DOTATATE uptakes in carotid and coronary arteries in patients with unstable CVD.¹⁸¹ Unlike ^{18}F -FDG, ^{68}Ga -DOTATATE does not have physiological myocardial uptake and therefore could potentially play a clinical role in detecting vulnerable plaque.

An alternative to ^{68}Ga , Copper-64 (^{64}Cu) complexed with the somatostatin analog (^{64}Cu -DOTATATE) has been used. ^{64}Cu has a shorter positron range and longer half-life. Thus, ^{64}Cu DOTATATE may have improved spatial resolution over that of ^{68}Ga -

DOTATATE. ^{64}Cu DOTATATE also showed positive uptake in carotid atherosclerotic lesions.¹⁸² ^{64}Cu -labeled DOTATATE uptake was positively linked to the expression of membrane receptor CD163, indicating that ^{64}Cu -labeled DOTATATE uptake was associated with hemorrhagic macrophage migration.

Translocator protein. Translocator protein 18kDa (TSPO), a peripheral-type benzodiazepine receptor, locates in peripheral tissue and the brain.¹⁸³ TSPO is a protein highly expressed in activated cells of the mononuclear phagocyte lineage.¹⁸⁴ Carbon-11 labeled [1-(2-chlorophenyl)-N-methyl-N-(1-methylpropyl)-3-isoquinolinecarboxamide] (^{11}C -PK11195) is a first specific ligand for TSPO, and its uptake has been revealed in symptomatic carotid atherosclerotic lesions.¹⁸⁵ However, ^{11}C -PK11195 has some limitations such as high non-specific binding and high lipophilicity. To overcome these limitations, we developed an ^{18}F -labeled TSPO ligand, *N*-benzyl-*N*-methyl-2-[7,8-dihydro-7-(2-[^{18}F]fluoroethyl)-8-oxo-2-phenyl-9*H*-purin-9-yl] acetamide (^{18}F -FEDAC). ^{18}F -FEDAC showed high in vitro binding affinity for TSPO with high selectivity.¹⁸⁶ ^{18}F -FEDAC was initially developed as a tracer for imaging brain inflammation, and subsequent study revealed that this tracer could potentially be used for imaging inflammation in peripheral organs.¹⁸⁷ Indeed, ^{18}F -FEDAC can be used to visualize lesions in rat liver.^{14,188} In a rat lung injury model, ^{18}F -FEDAC uptake increased with the progression of lung inflammation (Figure 11).¹⁸⁹ The uptake of ^{18}F -FEDAC in the heart of a rat was approximately twice as high as that in the lung.¹⁸⁷ With ^{18}F -FEDAC the uptake ratio for heart to lung is higher than that with ^{13}N -NH₃. The same is true for the heart-to-liver uptake ratio measured with each of these tracers respectively. However, uptake ratios are similar for heart to lung and heart to liver measured using ^{18}F -FEDAC and ^{18}F -FDG (Figure 12). In this regard, ^{18}F -FEDAC may have potential for detecting cardiac inflammatory lesions or vascular inflammatory lesions.

Fluorine-18 anion ($^{18}\text{F}^-$), which is administered as the sodium salt ^{18}F -NaF, has been used as a bone-imaging agent to detect metastatic bone lesions. Since $^{18}\text{F}^-$ accumulates in calcification lesions, it has also been used to evaluate the severity or disease activity of aortic stenosis.¹⁹⁰ During the progression of atherosclerosis, calcification may appear in intermediate lesions. In contrast, with inflammation, active calcification may appear during the later stages of disease progression. However, it is still important to detect actively progressing calcification, because this may be one of the signs of plaque rupture.¹⁹¹ Prospective studies with clinical outcomes are ongoing to assess whether coronary ^{18}F uptake represents a future cardiovascular risk.

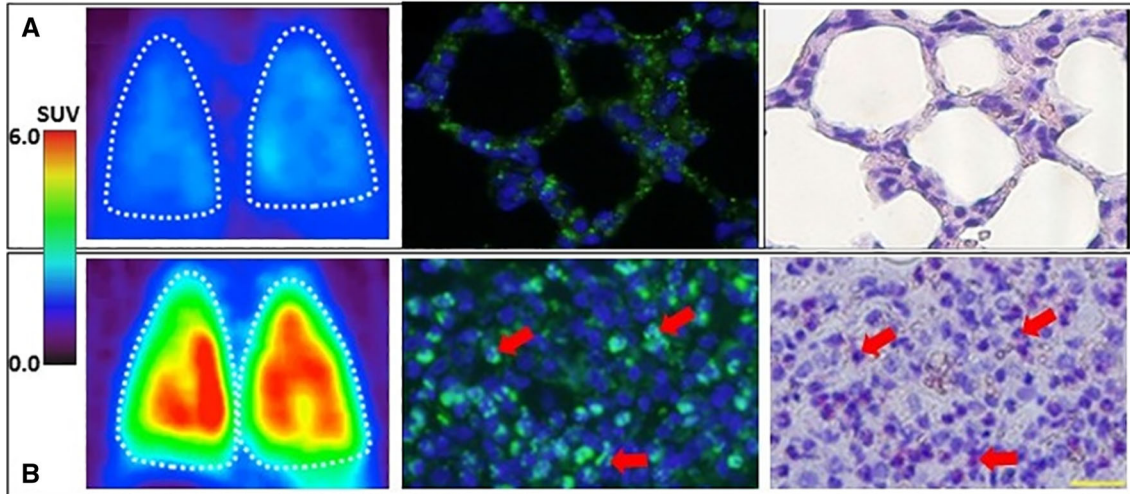


Figure 11. ^{18}F -FEDAC imaging a comparison between ^{18}F -FEDAC imaging and double staining of translocator protein (TSPO) for neutrophils. Arrows indicate examples of cells doubly positive for TSPO (green) and chloroacetate esterase (red spots) staining. Control group showed no positive ^{18}F -FEDAC uptake in either lung (A). No neutrophils were seen in the control. Lung injury model using lipopolysaccharide showed positive ^{18}F -FEDAC uptake in both lungs (B).

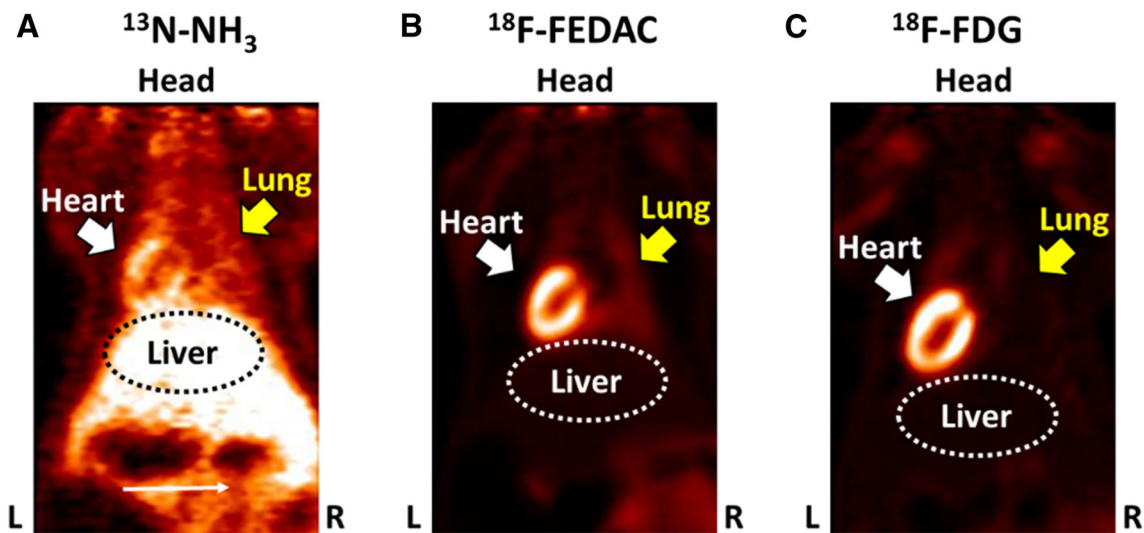


Figure 12. Histology showed leukocyte infiltration in the lung injury model. Scale bar: 20 μm . ^{18}F -FEDAC showed higher uptake ratios of heart/lung and heart/liver compared to those with ^{13}N - NH_3 and similar to that with ^{18}F -FDG. ^{18}F -FDG, ^{18}F -fluorodeoxyglucose; ^{18}F -FEDAC, *N*-benzyl-*N*-methyl-2-[7,8-dihydro-7-(2-[^{18}F]-fluoroethyl)-8-oxo-2-phenyl-9*H*-purin-9-yl] acetamide.

SUMMARY AND CONCLUSION

Nuclear cardiology using targeted tracers via SPECT and PET allows for diagnosis through non-invasive imaging. Not only myocardial perfusion but

also cardiac metabolism, sympathetic nervous system activity, and inflammatory disease are targeted by nuclear cardiology using specific radiopharmaceuticals.

Acknowledgments

The authors thank Ms. Mariko Yamasaki and Natuse Ito for their administrative assistance. This manuscript has been reviewed by a North American English-language professional editor, Ms. Holly Beanlands. The authors also thank Ms. Holly Beanlands for critical reading of the manuscript.

Disclosures

O. Manabe, T. Kikuchi, M. El Mahdiui, R. Nishii, M.-R. Zhang, E. Suzuki and K. Yoshinaga have nothing to disclose. A.J.H.A. Scholte is a Consultant for GE Healthcare and Toshiba Medical Systems.

Open Access

This article is distributed under the terms of the Creative Commons Attribution 4.0 International License (<http://creativecommons.org/licenses/by/4.0/>), which permits unrestricted use, distribution, and reproduction in any medium, provided you give appropriate credit to the original author(s) and the source, provide a link to the Creative Commons license, and indicate if changes were made.

References

1. Roth GA, Forouzanfar MH, Moran AE, Barber R, Nguyen G, Feigin VL, Naghavi M, Mensah GA, Murray CJ. Demographic and epidemiologic drivers of global cardiovascular mortality. *N Engl J Med* 2015;372:1333-41.
2. Bateman TM, Dilsizian V, Beanlands RS, DePuey EG, Heller GV, Wolinsky DA. American Society of Nuclear Cardiology and Society of Nuclear Medicine and Molecular Imaging Joint Position Statement on the Clinical Indications for Myocardial Perfusion PET. *J Nucl Med* 2016;57:1654-6.
3. Masuda A, Takeishi Y. Choosing the appropriate examination for diagnosis of stable ischemic heart disease. *Ann Nucl Cardiol* 2016;2:167-73.
4. Schindler T, Marashdeh W, Solnes L. Application of myocardial blood flow quantification in CAD patients. *Ann Nucl Cardiol* 2016;2:84-93.
5. Rauch B, Helus F, Grunze M, Braunwell E, Mall G, Hasselbach W, Kubler W. Kinetics of ¹³N-ammonia uptake in myocardial single cells indicating potential limitations in its applicability as a marker of myocardial blood flow. *Circulation* 1985;71:387-93.
6. Zaret BL, Strauss HW, Martin ND, Wells HP Jr, Flamm MD Jr. Noninvasive regional myocardial perfusion with radioactive potassium. Study of patients at rest, with exercise and during angina pectoris. *N Engl J Med* 1973;288:809-12.
7. Love WD, Romney RB, Burch GE. A comparison of the distribution of potassium and exchangeable rubidium in the organs of the dog, using rubidium. *Circ Res* 1954;2:112-22.
8. Bateman T. Current Status of myocardial perfusion PET in the United States. *Ann Nucl Cardiol* 2017;3:157-62.
9. Melon PG, Brihaye C, Degueldre C, Guillaume M, Czichosz R, Rigo P, Kulbertus HE, Comar D. Myocardial kinetics of potassium-38 in humans and comparison with copper-62-PTSM. *J Nucl Med* 1994;35:1116-22.
10. Tsan MF. Mechanism of gallium-67 accumulation in inflammatory lesions. *J Nucl Med* 1985;26:88-92.

11. Dweck MR, Jones C, Joshi NV, Fletcher AM, Richardson H, White A, Marsden M, Pessotto R, Clark JC, Wallace WA, Salter DM, McKillop G, van Beek EJ, Boon NA, Rudd JH, Newby DE. Assessment of valvular calcification and inflammation by positron emission tomography in patients with aortic stenosis. *Circulation* 2012;125:76-86.
12. Tamaki N, Morita K, Kuge Y, Tsukamoto E. The role of fatty acids in cardiac imaging. *J Nucl Med* 2000;41:1525-34.
13. Thackeray JT, Bengel FM. PET imaging of the autonomic nervous system. *Q J Nucl Med Mol Imaging* 2016;60:362-82.
14. Hatori A, Yui J, Xie L, Yamasaki T, Kumata K, Fujinaga M, Wakizaka H, Ogawa M, Nengaki N, Kawamura K, Zhang MR. Visualization of acute liver damage induced by cycloheximide in rats using PET with [¹⁸F]FEDAC, a radiotracer for translocator protein (18 kDa). *PLoS ONE* 2014;9:e86625.
15. Boersma HH, Kietselaer BL, Stolk LM, Bennaghmouch A, Hofstra L, Narula J, Heidendal GA, Reutelingsperger CP. Past, present, and future of annexin A5: From protein discovery to clinical applications. *J Nucl Med* 2005;46:2035-50.
16. Gould KL, Lipscomb K, Hamilton GW. Physiologic basis for assessing critical coronary stenosis. Instantaneous flow response and regional distribution during coronary hyperemia as measures of coronary flow reserve. *Am J Cardiol* 1974;33:87-94.
17. Yoshinaga K, Manabe O, Tamaki N. Physiological assessment of myocardial perfusion using nuclear cardiology would enhance coronary artery disease patient care: Which imaging modality is best for evaluation of myocardial ischemia? (SPECT-side). *Circ J* 2011;75:713-22 **discussion 731**.
18. Yoshinaga K, Manabe O, Tamaki N. Absolute quantification of myocardial blood flow. *J Nucl Cardiol* 2016. <https://doi.org/10.1007/s12350-016-0591-3>.
19. Manabe O, Naya M, Tamaki N. Feasibility of PET for the management of coronary artery disease: Comparison between CFR and FFR. *J Cardiol* 2017;2:135-40.
20. Maddahi J, Czernin J, Lazewatsky J, Huang SC, Dahlbom M, Schelbert H, Sparks R, Ehlgren A, Crane P, Zhu Q, Devine M, Phelps M. Phase I, first-in-human study of BMS747158, a novel ¹⁸F-labeled tracer for myocardial perfusion PET: Dosimetry, biodistribution, safety, and imaging characteristics after a single injection at rest. *J Nucl Med* 2011;52:1490-8.
21. Einstein AJ, Moser KW, Thompson RC, Cerqueira MD, Henzlova MJ. Radiation dose to patients from cardiac diagnostic imaging. *Circulation* 2007;116:1290-305.
22. Maddahi J, Packard RR. Cardiac PET perfusion tracers: Current status and future directions. *Semin Nucl Med* 2014;44:333-43.
23. Strauss HW, Harrison K, Langan JK, Lebowitz E, Pitt B. Thallium-201 for myocardial imaging. Relation of thallium-201 to regional myocardial perfusion. *Circulation* 1975;51:641-5.
24. Wackers FJ, Schoot JB, Sokole EB, Samson G, Niftrik GJ, Lie KI, Durrer D, Wellens HJ. Noninvasive visualization of acute myocardial infarction in man with thallium-201. *Br Heart J* 1975;37:741-4.
25. Atkins HL, Budinger TF, Lebowitz E, Ansari AN, Greene MW, Fairchild RG, Ellis KJ. Thallium-201 for medical use. Part 3: Human distribution and physical imaging properties. *J Nucl Med* 1977;18:133-40.
26. Krahwinkel W, Herzog H, Feinendegen LE. Pharmacokinetics of thallium-201 in normal individuals after routine myocardial scintigraphy. *J Nucl Med* 1988;29:1582-6.
27. Jain D, Thompson B, Wackers FJ, Zaret BL. Relevance of increased lung thallium uptake on stress imaging in patients with unstable angina and non-Q wave myocardial infarction: Results

- of the Thrombolysis in Myocardial Infarction (TIMI)-IIIB Study. *J Am Coll Cardiol* 1997;30:421-9.
28. Thompson RC, Cullom SJ. Issues regarding radiation dosage of cardiac nuclear and radiography procedures. *J Nucl Cardiol* 2006;13:19-23.
29. Otsuka R, Kubo N, Miyazaki Y, Kawahara M, Takaesu J, Fukuchi K. Current status of stress myocardial perfusion imaging pharmaceuticals and radiation exposure in Japan: Results from a nationwide survey. *J Nucl Cardiol* 2017. <https://doi.org/10.1007/s12350-017-0867-2>.
30. Iida H, Maruno H, Koshino K, Shimochi S, Temma T, Hutton B, Matsuo S. Quantitative assessment of regional myocardial blood flow with clinical SPECT. *Ann Nucl Cardiol* 2016;2:111-21.
31. Okada RD, Glover DK, Moffett JD, Beju D, Johnson G 3rd. Kinetics of technetium-^{99m}-teboroxime in reperfused nonviable myocardium. *J Nucl Med* 1997;38:274-9.
32. Beanlands RS, DeKemp RA, Harmsen E, Veinot JP, Hartman NG, Ruddy TD. Myocardial kinetics of technetium-^{99m} teboroxime in the presence of postischemic injury, necrosis and low flow reperfusion. *J Am Coll Cardiol* 1996;28:487-94.
33. Higley B, Smith FW, Smith T, Gemmell HG, Das Gupta P, Gvozdanovic DV, Graham D, Hinge D, Davidson J, Lahiri A. Technetium-^{99m}-1,2-bis[bis(2-ethoxyethyl) phosphino]ethane: human biodistribution, dosimetry and safety of a new myocardial perfusion imaging agent. *J Nucl Med* 1993;34:30-8.
34. Masuda A, Yoshinaga K, Naya M, Manabe O, Yamada S, Iwano H, Okada T, Katoh C, Takeishi Y, Tsutsui H, Tamaki N. Accelerated (^{99m}Tc)-sestamibi clearance associated with mitochondrial dysfunction and regional left ventricular dysfunction in reperfused myocardium in patients with acute coronary syndrome. *EJNMMI Res* 2016;6:41.
35. Wackers FJ, Berman DS, Maddahi J, Watson DD, Beller GA, Strauss HW, Boucher CA, Picard M, Holman BL, Fridrich R, et al. Technetium-^{99m} hexakis 2-methoxyisobutyl isonitrile: Human biodistribution, dosimetry, safety, and preliminary comparison to thallium-201 for myocardial perfusion imaging. *J Nucl Med* 1989;30:301-11.
36. Zaret BL, Rigo P, Wackers FJ, Hendel RC, Braat SH, Iskandrian AS, Sridhara BS, Jain D, Itti R, Serafini AN, et al. Myocardial perfusion imaging with ^{99m}Tc tetrofosmin. Comparison to 201Tl imaging and coronary angiography in a phase III multicenter trial. Tetrofosmin International Trial Study Group. *Circulation* 1995;91:313-9.
37. Flamen P, Bossuyt A, Franken PR. Technetium-99m-tetrofosmin in dipyridamole-stress myocardial SPECT imaging: Intraindividual comparison with technetium-^{99m}-sestamibi. *J Nucl Med* 1995;36:2009-15.
38. Munch G, Neverve J, Matsunari I, Schroter G, Schwaiger M. Myocardial technetium-^{99m}-tetrofosmin and technetium-^{99m}-sestamibi kinetics in normal subjects and patients with coronary artery disease. *J Nucl Med* 1997;38:428-32.
39. Yoshinaga K, Tomiyama Y, Suzuki E, Tamaki N. Myocardial blood flow quantification using positron-emission tomography: Analysis and practice in the clinical setting. *Circ J* 2013;77:1662-71.
40. Wang L, Wu D, Yang Y, Chen JJ, Lin CY, Hsu B, Fang W, Tang YD. Avoiding full corrections in dynamic SPECT images impacts the performance of SPECT myocardial blood flow quantitation. *J Nucl Cardiol* 2016. <https://doi.org/10.1007/s12350-016-0513-4>.
41. Wells RG, Timmins R, Klein R, Lockwood J, Marvin B, deKemp RA, Wei L, Ruddy TD. Dynamic SPECT measurement of absolute myocardial blood flow in a porcine model. *J Nucl Med* 2014;55:1685-91.
42. Yoshinaga K, Katoh C, Manabe O, Klein R, Naya M, Sakakibara M, Yamada S, Dekemp RA, Tsutsui H, Tamaki N. Incremental diagnostic value of regional myocardial blood flow quantification over relative perfusion imaging with generator-produced rubidium-82 PET. *Circ J* 2011;75:2628-34.
43. Giubbini R, Peli A, Milan E, Sciagra R, Camoni L, Albano D, Bertoli M, Bonacina M, Motta F, Statuto M, Rodella CA, De Agostini A, Calabretta R, Bertagna F, Italian Nuclear Cardiology G. Comparison between the summed difference score and myocardial blood flow measured by ¹³N-ammonia. *J Nucl Cardiol* 2017. <https://doi.org/10.1007/s12350-017-0789-z>.
44. Yoshinaga K, Tamaki N. Current status of nuclear cardiology in Japan: Ongoing efforts to improve clinical standards and to establish evidence. *J Nucl Cardiol* 2015;22:690-9.
45. Murthy VL, Naya M, Foster CR, Hainer J, Gaber M, Di Carli G, Blankstein R, Dorbala S, Sitek A, Pencina MJ, Di Carli MF. Improved cardiac risk assessment with noninvasive measures of coronary flow reserve. *Circulation* 2011;124:2215-24.
46. Taqueti VR, Hachamovitch R, Murthy VL, Naya M, Foster CR, Hainer J, Dorbala S, Blankstein R, Di Carli MF. Global coronary flow reserve is associated with adverse cardiovascular events independently of luminal angiographic severity and modifies the effect of early revascularization. *Circulation* 2015;131:19-27.
47. Naya M, Murthy VL, Taqueti VR, Foster CR, Klein J, Garber M, Dorbala S, Hainer J, Blankstein R, Resnic F, Di Carli MF. Preserved coronary flow reserve effectively excludes high-risk coronary artery disease on angiography. *J Nucl Med* 2014;55:248-55.
48. Naya M, Tamaki N, Tsutsui H. Coronary flow reserve estimated by positron emission tomography to diagnose significant coronary artery disease and predict cardiac events. *Circ J* 2015;79:15-23.
49. Ziadi MC, Dekemp RA, Williams K, Guo A, Renaud JM, Chow BJ, Klein R, Ruddy TD, Aung M, Garrard L, Beanlands RS. Does quantification of myocardial flow reserve using rubidium-82 positron emission tomography facilitate detection of multi-vessel coronary artery disease? *J Nucl Cardiol* 2012;19:670-80.
50. Klein R, Beanlands RS, deKemp RA. Quantification of myocardial blood flow and flow reserve: Technical aspects. *J Nucl Cardiol* 2010;17:555-70.
51. Packard RR, Huang SC, Dahlbom M, Czernin J, Maddahi J. Absolute quantitation of myocardial blood flow in human subjects with or without myocardial ischemia using dynamic flurpiridaz F 18 PET. *J Nucl Med* 2014;55:1438-44.
52. Yoshinaga K, Klein R, Tamaki N. Generator-produced rubidium-82 positron emission tomography myocardial perfusion imaging-From basic aspects to clinical applications. *J Cardiol* 2010;55:163-73.
53. Gould KL. Clinical cardiac PET using generator-produced Rb-82: A review. *Cardiovasc Interv Radiol* 1989;12:245-51.
54. Selwyn AP, Allan RM, L'Abbate A, Horlock P, Camici P, Clark J, O'Brien HA, Grant PM. Relation between regional myocardial uptake of rubidium-82 and perfusion: Absolute reduction of cation uptake in ischemia. *Am J Cardiol* 1982;50:112-21.
55. Yoshinaga K. Current clinical practice of nuclear cardiology in Japan. *Ann Nucl Cardiol* 2016;2:50-2.
56. Krivokapich J, Huang SC, Phelps ME, MacDonald NS, Shine KI. Dependence of ¹³NH₃ myocardial extraction and clearance on flow and metabolism. *Am J Physiol* 1982;242:H536-42.
57. Suda M, Onoguchi M, Tomiyama T, Ishihara K, Takahashi N, Sakurai M, Matsumoto K, Kumita S. The reproducibility of time-of-flight PET and conventional PET for the quantification of

- myocardial blood flow and coronary flow reserve with (13)N-ammonia. *J Nucl Cardiol* 2016;23:457-72.
58. Katoh C, Morita K, Shiga T, Kubo N, Nakada K, Tamaki N. Improvement of algorithm for quantification of regional myocardial blood flow using ¹⁵O-water with PET. *J Nucl Med* 2004;45:1908-16.
 59. Maruo A, Manabe O, Yoshinaga K, Naya M, Tomiyama Y, Oyama-Manabe N, Hirata K, Magota K, Tsutsui H, Katoh C, Tamaki N. Feasibility of quantifying myocardial blood flow with a shorter acquisition time using ¹⁵O-H₂O PET. *Ann Nucl Cardiol* 2016;2:30-7.
 60. Yoshinaga K, Manabe O, Katoh C, Chen L, Klein R, Naya M, deKemp RA, Williams K, Beanlands RS, Tamaki N. Quantitative analysis of coronary endothelial function with generator-produced ⁸²Rb PET: Comparison with ¹⁵O-labelled water PET. *Eur J Nucl Med Mol Imaging* 2010;37:2233-41.
 61. Tomiyama Y, Manabe O, Oyama-Manabe N, Naya M, Sugimori H, Hirata K, Mori Y, Tsutsui H, Kudo K, Tamaki N, Katoh C. Quantification of myocardial blood flow with dynamic perfusion 3.0 Tesla MRI: Validation with (15) O-water PET. *J Magn Reson Imaging* 2015;42:754-62.
 62. Mori Y, Manabe O, Naya M, Tomiyama Y, Yoshinaga K, Magota K, Oyama-Manabe N, Hirata K, Tsutsui H, Tamaki N, Katoh C. Improved spillover correction model to quantify myocardial blood flow by ¹¹C-acetate PET: Comparison with ¹⁵O-H₂O PET. *Ann Nucl Med* 2015;29:15-20.
 63. Naya M, Morita K, Yoshinaga K, Manabe O, Goto D, Hirata K, Katoh C, Tamaki N, Tsutsui H. Long-term smoking causes more advanced coronary endothelial dysfunction in middle-aged smokers compared to young smokers. *Eur J Nucl Med Mol Imaging* 2011;38:491-8.
 64. Danad I, Uusitalo V, Kero T, Saraste A, Raijmakers PG, Lamertsma AA, Heymans MW, Kajander SA, Pietila M, James S, Sorensen J, Knaapen P, Knuuti J. Quantitative assessment of myocardial perfusion in the detection of significant coronary artery disease: Cutoff values and diagnostic accuracy of quantitative [(15)O]H₂O PET imaging. *J Am Coll Cardiol* 2014;64:1464-75.
 65. Yu M, Nekolla SG, Schwaiger M, Robinson SP. The next generation of cardiac positron emission tomography imaging agents: Discovery of flurpiridaz F-18 for detection of coronary disease. *Semin Nucl Med* 2011;41:305-13.
 66. Huisman MC, Higuchi T, Reder S, Nekolla SG, Poethko T, Wester HJ, Ziegler SI, Casebier DS, Robinson SP, Schwaiger M. Initial characterization of an 18F-labeled myocardial perfusion tracer. *J Nucl Med* 2008;49:630-6.
 67. Berman DS, Maddahi J, Tamarappoo BK, Czernin J, Taillefer R, Udelson JE, Gibson CM, Devine M, Lazewatsky J, Bhat G, Washburn D. Phase II safety and clinical comparison with single-photon emission computed tomography myocardial perfusion imaging for detection of coronary artery disease: Flurpiridaz F 18 positron emission tomography. *J Am Coll Cardiol* 2013;61:469-77.
 68. Nekolla SG, Reder S, Saraste A, Higuchi T, Dzewas G, Preissel A, Huisman M, Poethko T, Schuster T, Yu M, Robinson S, Casebier D, Henke J, Wester HJ, Schwaiger M. Evaluation of the novel myocardial perfusion positron-emission tomography tracer 18F-BMS-747158-02: Comparison to ¹³N-ammonia and validation with microspheres in a pig model. *Circulation* 2009;119:2333-42.
 69. Manabe O, Yoshinaga K, Ohira H, Masuda A, Sato T, Tsujino I, Yamada A, Oyama-Manabe N, Hirata K, Nishimura M, Tamaki N. The effects of 18-h fasting with low-carbohydrate diet preparation on suppressed physiological myocardial (18)F-fluorodeoxyglucose (FDG) uptake and possible minimal effects of unfractionated heparin use in patients with suspected cardiac involvement sarcoidosis. *J Nucl Cardiol* 2016;23:244-52.
 70. Stanley WC, Recchia FA, Lopaschuk GD. Myocardial substrate metabolism in the normal and failing heart. *Physiol Rev* 2005;85:1093-129.
 71. Rosano GM, Fini M, Caminiti G, Barbaro G. Cardiac metabolism in myocardial ischemia. *Curr Pharm Des* 2008;14:2551-62.
 72. Neubauer S. The failing heart-an engine out of fuel. *N Engl J Med* 2007;356:1140-51.
 73. Matsumoto N, Hirayama A. Current Japanese Ministry of Health, Labor, and Welfare Approval of cardiac single photon emission computed tomography. *Ann Nucl Cardiol* 2015;1:108-9.
 74. Higashi MIY, Miyauchi H, Zaima N, Suzuki A, Li M, Kobayashi K, Naito H, Hirano K. Imaging modalities for Triglyceride deposit cardiomyovascularopathy. *Ann Nucl Cardiol* 2017;3:94-102.
 75. Knapp FF Jr, Goodman MM, Callahan AP, Kirsch G. Radioiodinated 15-(p-iodophenyl)-3,3-dimethylpentadecanoic acid: A useful new agent to evaluate myocardial fatty acid uptake. *J Nucl Med* 1986;27:521-31.
 76. Torizuka K, Yonekura Y, Nishimura T, Tamaki N, Uehara T, Ikekubo K, Hino M. A phase 1 study of beta-methyl-p-(123I)-iodophenyl-pentadecanoic acid (123I-BMIPP). *Kaku igaku Jpn J Nucl Med* 1991;28:681-90.
 77. Kurata C, Tawarahara K, Taguchi T, Aoshima S, Kobayashi A, Yamazaki N, Kawai H, Kaneko M. Myocardial emission computed tomography with iodine-123-labeled beta-methyl-branched fatty acid in patients with hypertrophic cardiomyopathy. *J Nucl Med* 1992;33:6-13.
 78. Tamaki N, Kawamoto M, Yonekura Y, Fujibayashi Y, Takahashi N, Konishi J, Nohara R, Kambara H, Kawai C, Ikekubo K, et al. Regional metabolic abnormality in relation to perfusion and wall motion in patients with myocardial infarction: Assessment with emission tomography using an iodinated branched fatty acid analog. *J Nucl Med* 1992;33:659-67.
 79. Kurisu S, Inoue I, Kawagoe T, Ishihara M, Shimatani Y, Nishioka K, Umemura T, Nakamura S, Yoshida M, Sato H. Myocardial perfusion and fatty acid metabolism in patients with tako-tsubo-like left ventricular dysfunction. *J Am Coll Cardiol* 2003;41:743-8.
 80. Dilsizian V, Bateman TM, Bergmann SR, Des Prez R, Magram MY, Goodbody AE, Babich JW, Udelson JE. Metabolic imaging with beta-methyl-p-[(123)I]-iodophenyl-pentadecanoic acid identifies ischemic memory after demand ischemia. *Circulation* 2005;112:2169-74.
 81. Knapp FF Jr, Kropp J. Iodine-123-labelled fatty acids for myocardial single-photon emission tomography: Current status and future perspectives. *Eur J Nucl Med* 1995;22:361-81.
 82. Yoshizumi T, Nozaki S, Fukuchi K, Yamasaki K, Fukuchi T, Maruyama T, Tomiyama Y, Yamashita S, Nishimura T, Matsuzawa Y. Pharmacokinetics and metabolism of 123I-BMIPP fatty acid analog in healthy and CD36-deficient subjects. *J Nucl Med* 2000;41:1134-8.
 83. Cavelliers V, Franken PR, Lin Q, Mokler FT, Luo H, Knapp FF Jr. Intra-individual comparison of 3(R)-BMIPP and 3(S)-BMIPP isomers in humans. *J Nucl Med* 1998;39:1672-5.
 84. Fujibayashi Y, Yonekura Y, Takemura Y, Wada K, Matsumoto K, Tamaki N, Yamamoto K, Konishi J, Yokoyama A. Myocardial accumulation of iodinated beta-methyl-branched fatty acid analogue, iodine-125-15-(p-iodophenyl)-3-(R, S)methylpentadecanoic acid (BMIPP), in relation to ATP concentration. *J Nucl Med* 1990;31:1818-22.

85. Dudczak R, Schmoliner R, Angelberger P, Knapp FF, Goodman MM. Structurally modified fatty acids: Clinical potential as tracers of metabolism. *Eur J Nucl Med* 1986;12:S45-8.
86. Gunnarsson M, Stenstrom K, Leide-Svegborn S, Faarinen M, Magnusson CE, Aberg M, Skog G, Hellborg R, Mattsson S. Biokinetics and radiation dosimetry for patients undergoing a glycerol tri[1-14C]oleate fat malabsorption breath test. *Appl Radiat Isotopes* 2003;58:517-26.
87. Reske SN, Sauer W, Machulla HJ, Knust J, Winkler C. Metabolism of 15 (p 123I iodophenyl)-pentadecanoic acid in heart muscle and noncardiac tissues. *Eur J Nucl Med* 1985;10:228-34.
88. Reske SN, Sauer W, Machulla HJ, Winkler C. 15(p-[123I]iodophenyl)pentadecanoic acid as tracer of lipid metabolism: Comparison with [1-14C]palmitic acid in murine tissues. *J Nucl Med* 1984;25:1335-42.
89. Torizuka K, Yonekura Y, Nishimura T, Tamaki N, Uehara T. Phase 2 study of beta-methyl-p-(123I)-iodophenyl-pentadecanoic acid, a myocardial imaging agent for evaluating myocardial fatty acid metabolism. *Kaku igaku Jpn J Nucl Med* 1992;29:305-17.
90. De Geeter F, Franken PR, Knapp FF Jr, Bossuyt A. Relationship between blood flow and fatty acid metabolism in subacute myocardial infarction: A study by means of ^{99m}Tc-Sestamibi and ¹²³I-beta-methyl-iodo-phenyl pentadecanoic acid. *Eur J Nucl Med* 1994;21:283-91.
91. Kawai Y, Tsukamoto E, Nozaki Y, Morita K, Sakurai M, Tamaki N. Significance of reduced uptake of iodinated fatty acid analogue for the evaluation of patients with acute chest pain. *J Am Coll Cardiol* 2001;38:1888-94.
92. Yoshinaga K, Naya M, Shiga T, Suzuki E, Tamaki N. Ischaemic memory imaging using metabolic radiopharmaceuticals: Overview of clinical settings and ongoing investigations. *Eur J Nucl Med Mol Imaging* 2014;41:384-93.
93. Fukuzawa S, Ozawa S, Shimada K, Sugioka J, Inagaki M. Prognostic values of perfusion-metabolic mismatch in TI-201 and BMIPP scintigraphic imaging in patients with chronic coronary artery disease and left ventricular dysfunction undergoing revascularization. *Ann Nucl Med* 2002;16:109-15.
94. Tillisch J, Brunken R, Marshall R, Schwaiger M, Mandelkern M, Phelps M, Schelbert H. Reversibility of cardiac wall-motion abnormalities predicted by positron tomography. *N Engl J Med* 1986;314:884-8.
95. Landau BR, Spring-Robinson CL, Muzic RF Jr, Rachdaoui N, Rubin D, Berridge MS, Schumann WC, Chandramouli V, Kern TS, Ismail-Beigi F. 6-Fluoro-6-deoxy-D-glucose as a tracer of glucose transport. *Am J Physiol Endocrinol Metab* 2007;293:E237-45.
96. Hasegawa S, Kusuoka H, Uehara T, Yamaguchi H, Hori M, Nishimura T. Glucose tolerance and myocardial F-18 fluorodeoxyglucose uptake in normal regions in coronary heart disease patients. *Ann Nucl Med* 1998;12:363-8.
97. Vitale GD, deKemp RA, Ruddy TD, Williams K, Beanlands RS. Myocardial glucose utilization and optimization of (18)F-FDG PET imaging in patients with non-insulin-dependent diabetes mellitus, coronary artery disease, and left ventricular dysfunction. *J Nucl Med* 2001;42:1730-6.
98. Tamaki N, Yonekura Y, Yamashita K, Saji H, Magata Y, Senda M, Konishi Y, Hirata K, Ban T, Konishi J. Positron emission tomography using fluorine-18 deoxyglucose in evaluation of coronary artery bypass grafting. *Am J Cardiol* 1989;64:860-5.
99. Kistrieva-Ware Z, Coggan AR, Sharp TL, Dence CS, Gropler RJ, Herrero P. Assessment of myocardial triglyceride oxidation with PET and 11C-palmitate. *J Nucl Cardiol* 2009;16:411-21.
100. Taylor M, Wallhaus TR, Degrado TR, Russell DC, Stanko P, Nickles RJ, Stone CK. An evaluation of myocardial fatty acid and glucose uptake using PET with [18F]fluoro-6-thia-heptadecanoic acid and [18F]FDG in Patients with Congestive Heart Failure. *J Nucl Med* 2001;42:55-62.
101. Maki MT, Haaparanta M, Nuutila P, Oikonen V, Luotolahti M, Eskola O, Knutti JM. Free fatty acid uptake in the myocardium and skeletal muscle using fluorine-18-fluoro-6-thia-heptadecanoic acid. *J Nucl Med* 1998;39:1320-7.
102. Ohira H, deKemp R, Pena E, Davies RA, Stewart DJ, Chandy G, Contreras-Dominguez V, Dennie C, Mc Ardle B, Mc Klein R, Renaud JM, DaSilva JN, Pugliese C, Dunne R, Beanlands R, Mielniczuk LM. Shifts in myocardial fatty acid and glucose metabolism in pulmonary arterial hypertension: A potential mechanism for a maladaptive right ventricular response. *Eur Heart J Cardiovasc Imaging* 2016;17:1424-31.
103. Nesterov SV, Turta O, Han C, Maki M, Lisinen I, Tuunanen H, Knutti J. C-11 acetate has excellent reproducibility for quantification of myocardial oxidative metabolism. *Eur Heart J Cardiovasc Imaging* 2015;16:500-6.
104. Tamaki N, Magata Y, Takahashi N, Kawamoto M, Torizuka T, Yonekura Y, Nishizawa S, Sadato N, Tadamura E, Ono S, et al. Myocardial oxidative metabolism in normal subjects in fasting, glucose loading and dobutamine infusion states. *Ann Nucl Med* 1992;6:221-8.
105. Brown M, Marshall DR, Sobel BE, Bergmann SR. Delineation of myocardial oxygen utilization with carbon-11-labeled acetate. *Circulation* 1987;76:687-96.
106. Buxton DB, Schwaiger M, Nguyen A, Phelps ME, Schelbert HR. Radiolabeled acetate as a tracer of myocardial tricarboxylic acid cycle flux. *Circ Res* 1988;63:628-34.
107. Walsh MN, Geltman EM, Brown MA, Henes CG, Weinheimer CJ, Sobel BE, Bergmann SR. Noninvasive estimation of regional myocardial oxygen consumption by positron emission tomography with carbon-11 acetate in patients with myocardial infarction. *J Nucl Med* 1989;30:1798-808.
108. Kalff V, Hicks RJ, Hutchins G, Topol E, Schwaiger M. Use of carbon-11 acetate and dynamic positron emission tomography to assess regional myocardial oxygen consumption in patients with acute myocardial infarction receiving thrombolysis or coronary angioplasty. *Am J Cardiol* 1993;71:529-35.
109. Wu YW, Naya M, Tsukamoto T, Komatsu H, Morita K, Yoshinaga K, Kuge Y, Tsutsui H, Tamaki N. Heterogeneous reduction of myocardial oxidative metabolism in patients with ischemic and dilated cardiomyopathy using C-11 acetate PET. *Circ J* 2008;72:786-92.
110. Tadamura E, Tamaki N, Matsumori A, Magata Y, Yonekura Y, Nohara R, Sasayama S, Yoshibayashi M, Kamiya T, Konishi J. Myocardial metabolic changes in hypertrophic cardiomyopathy. *J Nucl Med* 1996;37:572-7.
111. Beanlands RS, Nahmias C, Gordon E, Coates G, deKemp R, Firnao G, Fallen E. The effects of beta(1)-blockade on oxidative metabolism and the metabolic cost of ventricular work in patients with left ventricular dysfunction: A double-blind, placebo-controlled, positron-emission tomography study. *Circulation* 2000;102:2070-5.
112. Hall AB, Ziadi MC, Leech JA, Chen SY, Burwash IG, Renaud J, deKemp RA, Haddad H, Mielniczuk LM, Yoshinaga K, Guo A, Chen L, Walter O, Garrard L, DaSilva JN, Floras JS, Beanlands RS. Effects of short-term continuous positive airway pressure on myocardial sympathetic nerve function and energetics in patients with heart failure and obstructive sleep apnea: A randomized study. *Circulation* 2014;130:892-901.
113. Wong YY, Rajmakers P, van Campen J, van der Laarse WJ, Knaapen P, Lubberink M, Ruiters G, Vonk Noordegraaf A, Lammertsma AA. 11C-Acetate clearance as an index of oxygen

- consumption of the right myocardium in idiopathic pulmonary arterial hypertension: A validation study using ¹⁵O-labeled tracers and PET. *J Nucl Med* 2013;54:1258-62.
114. Stolen KQ, Kemppainen J, Ukkonen H, Kalliokoski KK, Luotolahti M, Lehtikoinen P, Hamalainen H, Salo T, Airaksinen KE, Nuutila P, Knuuti J. Exercise training improves biventricular oxidative metabolism and left ventricular efficiency in patients with dilated cardiomyopathy. *J Am Coll Cardiol* 2003;41:460-7.
 115. Hicks RJ, Kalff V, Savas V, Starling MR, Schwaiger M. Assessment of right ventricular oxidative metabolism by positron emission tomography with C-11 acetate in aortic valve disease. *Am J Cardiol* 1991;67:753-7.
 116. Yoshinaga K, Ohira H, Tsujino I, Oyama-Manabe N, Mielniczuk L, Beanlands RS, Katoh C, Kasai K, Manabe O, Sato T, Fujii S, Ito YM, Tomiyama Y, Nishimura M, Tamaki N. Attenuated right ventricular energetics evaluated using (1)(1)C-acetate PET in patients with pulmonary hypertension. *Eur J Nucl Med Mol Imaging* 2014;41:1240-50.
 117. Francis GS. Modulation of peripheral sympathetic nerve transmission. *J Am Coll Cardiol* 1988;12:250-4.
 118. Melon PG, Nguyen N, DeGrado TR, Mangner TJ, Wieland DM, Schwaiger M. Imaging of cardiac neuronal function after cocaine exposure using carbon-11 hydroxyephedrine and positron emission tomography. *J Am Coll Cardiol* 1994;23:1693-9.
 119. Nomura Y, Matsunari I, Takamatsu H, Murakami Y, Matsuya T, Taki J, Nakajima K, Nekolla SG, Chen WP, Kajinami K. Quantitation of cardiac sympathetic innervation in rabbits using 11C-hydroxyephedrine PET: Relation to 123I-MIBG uptake. *Eur J Nucl Med Mol Imaging* 2006;33:871-8.
 120. Mitrani RD, Klein LS, Miles WM, Hackett FK, Burt RW, Wellman HN, Zipes DP. Regional cardiac sympathetic denervation in patients with ventricular tachycardia in the absence of coronary artery disease. *J Am Coll Cardiol* 1993;22:1344-53.
 121. Tsukamoto T, Morita K, Naya M, Inubushi M, Katoh C, Nishijima K, Kuge Y, Okamoto H, Tsutsui H, Tamaki N. Decreased myocardial beta-adrenergic receptor density in relation to increased sympathetic tone in patients with nonischemic cardiomyopathy. *J Nucl Med* 2007;48:1777-82.
 122. Brunner-La Rocca HP, Esler MD, Jennings GL, Kaye DM. Effect of cardiac sympathetic nervous activity on mode of death in congestive heart failure. *Eur Heart J* 2001;22:1136-43.
 123. Paul M, Schafers M, Kies P, Acil T, Schafers K, Breithardt G, Schober O, Wichter T. Impact of sympathetic innervation on recurrent life-threatening arrhythmias in the follow-up of patients with idiopathic ventricular fibrillation. *Eur J Nucl Med Mol Imaging* 2006;33:866-70.
 124. Nakata T, Miyamoto K, Doi A, Sasao H, Wakabayashi T, Kobayashi H, Tsuchihashi K, Shimamoto K. Cardiac death prediction and impaired cardiac sympathetic innervation assessed by MIBG in patients with failing and nonfailing hearts. *J Nucl Cardiol* 1998;5:579-90.
 125. Nakata T, Nakajima K, Yamashina S, Yamada T, Momose M, Kasama S, Matsui T, Matsuo S, Travin MI, Jacobson AF. A pooled analysis of multicenter cohort studies of (123)I-mIBG imaging of sympathetic innervation for assessment of long-term prognosis in heart failure. *JACC Cardiovasc Imaging* 2013;6:772-84.
 126. Nakajima K, Scholte A, Nakata T, Dimitriu-Leen AC, Chikamori T, Vitola JV, Yoshinaga K. Cardiac sympathetic nervous system imaging with ¹²³I-meta-iodobenzylguanidine: Perspectives from Japan and Europe. *J Nucl Cardiol* 2017;24:952-60.
 127. Nakajima K, Nakata T. Cardiac ¹²³I-MIBG imaging for clinical decision making: 22-year Experience in Japan. *J Nucl Med* 2015;56:11S-9S.
 128. Kline RC, Swanson DP, Wieland DM, Thrall JH, Gross MD, Pitt B, Beierwaltes WH. Myocardial imaging in man with I-123 meta-iodobenzylguanidine. *J Nucl Med* 1981;22:129-32.
 129. Bengel FM. Imaging targets of the sympathetic nervous system of the heart: Translational considerations. *J Nucl Med* 2011;52:1167-70.
 130. Lautamaki R, Tipre D, Bengel FM. Cardiac sympathetic neuronal imaging using PET. *Eur J Nucl Med Mol Imaging* 2007;34:S74-85.
 131. Henzlova MJ, Duvall WL, Einstein AJ, Travin MI, Verberne HJ. ASNC imaging guidelines for SPECT nuclear cardiology procedures: Stress, protocols, and tracers. *J Nucl Cardiol* 2016;23:606-39.
 132. Nakajima K, Okuda K, Matsuo S, Yoshita M, Taki J, Yamada M, Kinuya S. Standardization of metaiodobenzylguanidine heart to mediastinum ratio using a calibration phantom: Effects of correction on normal databases and a multicentre study. *Eur J Nucl Med Mol Imaging* 2012;39:113-9.
 133. Nakajima K, Scholte JHAA, Nakata T, Dimitriu-Leen AC, Chikamori T, Yoshinaga K. Cardiac sympathetic nervous system imaging with ¹²³I-meta-iodobenzylguanidine: Perspectives from Japan and Europe. *Ann Nucl Cardiol* 2017;24:952-60.
 134. Thackeray JT, Bengel FM. Assessment of cardiac autonomic neuronal function using PET imaging. *J Nucl Cardiol* 2013;20:150-65.
 135. Fallavollita JA, Heavey BM, Luisi AJ Jr, Michalek SM, Baldwa S, Mashtare TL Jr, Hutson AD, Dekemp RA, Haka MS, Sajjad M, Cimato TR, Curtis AB, Cain ME, Cauty JM Jr. Regional myocardial sympathetic denervation predicts the risk of sudden cardiac arrest in ischemic cardiomyopathy. *J Am Coll Cardiol* 2014;63:141-9.
 136. Bulow HP, Stahl F, Lauer B, Nekolla SG, Schuler G, Schwaiger M, Bengel FM. Alterations of myocardial presynaptic sympathetic innervation in patients with multi-vessel coronary artery disease but without history of myocardial infarction. *Nucl Med Commun* 2003;24:233-9.
 137. Harms HJ, Lubberink M, de Haan S, Knaapen P, Huisman MC, Schuit RC, Windhorst AD, Allaart CP, Lammertsma AA. Use of a single 11C-Meta-hydroxyephedrine scan for assessing flow-innervation mismatches in patients with ischemic cardiomyopathy. *J Nucl Med* 2015;56:1706-11.
 138. Pietila M, Malmiemiemi K, Ukkonen H, Saraste M, Nagren K, Lehtikoinen P, Voipio-Pulkki LM. Reduced myocardial carbon-11 hydroxyephedrine retention is associated with poor prognosis in chronic heart failure. *Eur J Nucl Med* 2001;28:373-6.
 139. Bengel FM, Permanetter B, Ungerer M, Nekolla SG, Schwaiger M. Alterations of the sympathetic nervous system and metabolic performance of the cardiomyopathic heart. *Eur J Nucl Med Mol Imaging* 2002;29:198-202.
 140. Mazzadi AN, Andre-Fouet X, Duisit J, Gebuhrer V, Costes N, Chevalier P, Rodriguez C, Schott JJ, Le Marec H, Guicheney P, Le Bars D, Janier M. Cardiac retention of [11C]HED in genotyped long QT patients: a potential amplifier role for severity of the disease. *Am J Physiol Heart Circ Physiol* 2003;285:H1286-93.
 141. Olgin JE, Sih HJ, Hanish S, Jayachandran JV, Wu J, Zheng QH, Winkle W, Mulholland GK, Zipes DP, Hutchins G. Heterogeneous atrial denervation creates substrate for sustained atrial fibrillation. *Circulation* 1998;98:2608-14.
 142. Allman KC, Wieland DM, Muzik O, DeGrado TR, Wolfe ER Jr, Schwaiger M. Carbon-11 hydroxyephedrine with positron emission tomography for serial assessment of cardiac adrenergic neuronal function after acute myocardial infarction in humans. *J Am Coll Cardiol* 1993;22:368-75.

143. Aoki H, Matsunari I, Nomura Y, Fujita W, Komatsu R, Miyazaki Y, Nekolla SG, Kajinami K. Myocardial sympathetic innervation, function, and oxidative metabolism in non-infarcted myocardium in patients with prior myocardial infarction. *Ann Nucl Med* 2013;27:523-31.
144. Allman KC, Stevens MJ, Wieland DM, Hutchins GD, Wolfe ER Jr, Greene DA, Schwaiger M. Noninvasive assessment of cardiac diabetic neuropathy by carbon-11 hydroxyephedrine and positron emission tomography. *J Am Coll Cardiol* 1993;22:1425-32.
145. Stevens MJ, Raffel DM, Allman KC, Schwaiger M, Wieland DM. Regression and progression of cardiac sympathetic dysinnervation complicating diabetes: An assessment by C-11 hydroxyephedrine and positron emission tomography. *Metabolism* 1999;48:92-101.
146. Aikawa T, Naya M, Obara M, Manabe O, Tomiyama Y, Magota K, Yamada S, Katoh C, Tamaki N, Tsutsui H. Impaired myocardial sympathetic innervation is associated with diastolic dysfunction in heart failure with preserved ejection fraction: 11C-Hydroxyephedrine PET study. *J Nucl Med* 2017;58:784-90.
147. Sinusas AJ, Lazewatsky J, Brunetti J, Heller G, Srivastava A, Liu YH, Sparks R, Pureskiy A, Lin SF, Crane P, Carson RE, Lee LV. Biodistribution and radiation dosimetry of LMI1195: First-in-human study of a novel ¹⁸F-labeled tracer for imaging myocardial innervation. *J Nucl Med* 2014;55:1445-51.
148. Eskola O, Gronroos T, Bergman J, Haaparanta M, Marjamaki P, Lehtikoinen P, Forsback S, Langer O, Hinnen F, Dolle F, Halldin C, Solin O. A novel electrophilic synthesis and evaluation of medium specific radioactivity (1R,2S)-4-[¹⁸F]fluorometaraminol, a tracer for the assessment of cardiac sympathetic nerve integrity with PET. *Nucl Med Biol* 2004;31:103-10.
149. Raffel DM, Corbett JR, del Rosario RB, Mukhopadhyay SK, Gildersleeve DL, Rose P, Wieland DM. Sensitivity of [¹¹C]phenylephrine kinetics to monoamine oxidase activity in normal human heart. *J Nucl Med* 1999;40:232-8.
150. Goldstein DS, Eisenhofer G, Dunn BB, Armando I, Lenders J, Grossman E, Holmes C, Kirk KL, Bacharach S, Adams R, et al. Positron emission tomographic imaging of cardiac sympathetic innervation using 6-[¹⁸F]fluorodopamine: Initial findings in humans. *J Am Coll Cardiol* 1993;22:1961-71.
151. Munch G, Nguyen NT, Nekolla S, Ziegler S, Muzik O, Chakraborty P, Wieland DM, Schwaiger M. Evaluation of sympathetic nerve terminals with [(11)C]epinephrine and [(11)C]hydroxyephedrine and positron emission tomography. *Circulation* 2000;101:516-23.
152. Salinas C, Muzic RF Jr, Berridge M, Ernsberger P. PET imaging of myocardial beta-adrenergic receptors with fluorocarazolol: Lack of interference by endogenous catecholamines. *J Cardiovasc Pharmacol* 2005;46:222-31.
153. Naya M, Tsukamoto T, Morita K, Katoh C, Nishijima K, Komatsu H, Yamada S, Kuge Y, Tamaki N, Tsutsui H. Myocardial beta-adrenergic receptor density assessed by 11C-CGP12177 PET predicts improvement of cardiac function after carvedilol treatment in patients with idiopathic dilated cardiomyopathy. *J Nucl Med* 2009;50:220-5.
154. de Jong RM, Willemsen AT, Slart RH, Blanksma PK, van Waarde A, Cornel JH, Vaalburg W, van Veldhuisen DJ, Elsinga PH. Myocardial beta-adrenoceptor downregulation in idiopathic dilated cardiomyopathy measured in vivo with PET using the new radioligand (S)-[¹¹C]CGP12388. *Eur J Nucl Med Mol Imaging* 2005;32:443-7.
155. Bengel FM, Higuchi T, Javadi MS, Lautamaki R. Cardiac positron emission tomography. *J Am Coll Cardiol* 2009;54:1-15.
156. Petrou M, Frey KA, Kilbourn MR, Scott PJ, Raffel DM, Bohnen NI, Muller ML, Albin RL, Koeppe RA. In vivo imaging of human cholinergic nerve terminals with (-)-5-(18)F-fluoroethoxybenzovesamicol: Biodistribution, dosimetry, and tracer kinetic analyses. *J Nucl Med* 2014;55:396-404.
157. Mulholland GK, Otto CA, Jewett DM, Kilbourn MR, Koeppe RA, Sherman PS, Petry NA, Carey JE, Atkinson ER, Archer S, et al. Synthesis, rodent biodistribution, dosimetry, metabolism, and monkey images of carbon-11-labeled (+)-2 alpha-tropanyl benzilate: A central muscarinic receptor imaging agent. *J Nucl Med* 1992;33:423-30.
158. Futamatsu H, Suzuki J, Adachi S, Okada H, Otomo K, Ohara T, Hashimoto Y, Kakuta T, Iesaka Y, Yamaguchi H, Sakurada H, Sato A, Obayashi T, Niwa A, Hirao K, Isobe M. Utility of gallium-67 scintigraphy for evaluation of cardiac sarcoidosis with ventricular tachycardia. *Int J Cardiovasc Imaging* 2006;22:443-8.
159. Palestro CJ. The current role of gallium imaging in infection. *Semin Nucl Med* 1994;24:128-41.
160. Love C, Palestro CJ. Radionuclide imaging of infection. *J Nucl Med Technol* 2004;32:47-57.
161. Hung MY, Hung MJ, Cheng CW. Use of gallium 67 scintigraphy to differentiate acute myocarditis from acute myocardial infarction. *Tex Heart Inst J* 2007;34:305-9.
162. Terasaki F, Yoshinaga K. New guidelines for diagnosis of cardiac sarcoidosis in Japan. *Ann Nucl Cardiol* 2017;3:42-5.
163. Ishimaru S, Tsujino I, Takei T, Tsukamoto E, Sakaue S, Kamigaki M, Ito N, Ohira H, Ikeda D, Tamaki N, Nishimura M. Focal uptake on ¹⁸F-fluoro-2-deoxyglucose positron emission tomography images indicates cardiac involvement of sarcoidosis. *Eur Heart J* 2005;26:1538-43.
164. Cerqueira MD, Jacobson AF. Indium-111 leukocyte scintigraphic detection of myocardial abscess formation in patients with endocarditis. *J Nucl Med* 1989;30:703-6.
165. Erba PA, Sollini M, Conti U, Bandera F, Tascini C, De Tommasi SM, Zucchelli G, Doria R, Menichetti F, Bongiorno MG, Lazzeri E, Mariani G. Radiolabeled WBC scintigraphy in the diagnostic workup of patients with suspected device-related infections. *JACC Cardiovasc Imaging* 2013;6:1075-86.
166. Rouzet F, Chequer R, Benali K, Lepage L, Ghodbane W, Duval X, Iung B, Vahanian A, Le Guludec D, Hyafil F. Respective performance of 18F-FDG PET and radiolabeled leukocyte scintigraphy for the diagnosis of prosthetic valve endocarditis. *J Nucl Med* 2014;55:1980-5.
167. Libby P, Nahrendorf M, Swirski FK. Leukocytes link local and systemic inflammation in ischemic cardiovascular disease: An expanded "cardiovascular continuum". *J Am Coll Cardiol* 2016;67:1091-103.
168. Kietselaer BL, Reutelingsperger CP, Heidendal GA, Daemen MJ, Mess WH, Hofstra L, Narula J. Noninvasive detection of plaque instability with use of radiolabeled annexin A5 in patients with carotid-artery atherosclerosis. *N Engl J Med* 2004;350:1472-3.
169. Yamashita A, Zhao Y, Zhao S, Matsuura Y, Sugita C, Iwakiri T, Okuyama N, Ohe K, Koshimoto C, Kawai K, Tamaki N, Kuge Y, Asada Y. Arterial (18)F-fluorodeoxyglucose uptake reflects balloon catheter-induced thrombus formation and tissue factor expression via nuclear factor-kappaB in rabbit atherosclerotic lesions. *Circ J* 2013;77:2626-35.
170. Ohira H, Tsujino I, Yoshinaga K. (1)(8)F-Fluoro-2-deoxyglucose positron emission tomography in cardiac sarcoidosis. *Eur J Nucl Med Mol Imaging* 2011;38:1773-83.
171. Manabe O, Oyama-Manabe N, Ohira H, Tsutsui H, Tamaki N. Multimodality evaluation of cardiac sarcoidosis. *J Nucl Cardiol* 2012;19:621-4.
172. Kong EJ, Lee SH, Cho IH. Myocardial fibrosis in hypertrophic cardiomyopathy demonstrated by integrated cardiac F-18 FDG PET/MR. *Nucl Med Mol Imaging* 2013;47:196-200.

173. Masuda A, Manabe O, Oyama-Manabe N, Naya M, Obara M, Sakakibara M, Hirata K, Yamada S, Naka T, Tsutsui H, Tamaki N. Cardiac fibroma with high 18F-FDG uptake mimicking malignant tumor. *J Nucl Cardiol* 2017;24:323-4.
174. Kikuchi Y, Oyama-Manabe N, Manabe O, Naya M, Ito YM, Hatanaka KC, Tsutsui H, Terae S, Tamaki N, Shirato H. Imaging characteristics of cardiac dominant diffuse large B-cell lymphoma demonstrated with MDCT and PET/CT. *Eur J Nucl Med Mol Imaging* 2013;40:1337-44.
175. Aikawa T, Naya M, Manabe O, Obara M, Matsushima S, Tamaki N, Tsutsui H. Incidental focal myocardial (18)F-FDG uptake indicating asymptomatic coronary artery disease. *J Nucl Cardiol* 2016;23:596-8.
176. Gormsen LC, Haraldsen A, Kramer S, Dias AH, Kim WY, Borghammer P. A dual tracer (68)Ga-DOTANOC PET/CT and (18)F-FDG PET/CT pilot study for detection of cardiac sarcoidosis. *EJNMMI Res* 2016;6:52.
177. Norikane T, Yamamoto Y, Maeda Y, Noma T, Nishiyama Y. 18F-FLT PET imaging in a patient with sarcoidosis with cardiac involvement. *Clin Nucl Med* 2015;40:433-4.
178. Lapa C, Reiter T, Kircher M, Schirbel A, Werner RA, Pelzer T, Pizarro C, Skowasch D, Thomas L, Schlesinger-Irsch U, Thomas D, Bundschuh RA, Bauer WR, Gartner FC. Somatostatin receptor based PET/CT in patients with the suspicion of cardiac sarcoidosis: An initial comparison to cardiac MRI. *Oncotarget* 2016;7:77807-14.
179. Manabe O, Hirata K, Shozo O, Shiga T, Uchiyama Y, Kobayashi K, Watanabe S, Toyonaga T, Kikuchi H, Oyama-Manabe N, Tamaki N. 18F-fluoromisonidazole (FMISO) PET may have the potential to detect cardiac sarcoidosis. *J Nucl Cardiol* 2017;24:329-31.
180. Schatka I, Wollenweber T, Haense C, Brunz F, Gratz KF, Bengel FM. Peptide receptor-targeted radionuclide therapy alters inflammation in atherosclerotic plaques. *J Am Coll Cardiol* 2013;62:2344-5.
181. Tarkin JM, Joshi FR, Evans NR, Chowdhury MM, Figg NL, Shah AV, Starks LT, Martin-Garrido A, Manavaki R, Yu E, Kuc RE, Grassi L, Kreuzhuber R, Kostadima MA, Frontini M, Kirkpatrick PJ, Coughlin PA, Gopalan D, Fryer TD, Buscombe JR, Groves AM, Ouwehand WH, Bennett MR, Warburton EA, Davenport AP, Rudd JH. Detection of Atherosclerotic Inflammation by 68Ga-DOTATATE PET Compared to [18F]FDG PET Imaging. *J Am Coll Cardiol* 2017;69:1774-91.
182. Pedersen SF, Sandholt BV, Keller SH, Hansen AE, Clemmensen AE, Sillesen H, Hojgaard L, Ripa RS, Kjaer A. ⁶⁴Cu-DOTA-TATE PET/MRI for detection of activated macrophages in carotid atherosclerotic plaques: Studies in patients undergoing endarterectomy. *Arterioscler Thromb Vasc Biol* 2015;35:1696-703.
183. Yui J, Maeda J, Kumata K, Kawamura K, Yanamoto K, Hatori A, Yamasaki T, Nengaki N, Higuchi M, Zhang MR. 18F-FEAC and 18F-FEDAC: PET of the monkey brain and imaging of translocator protein (18 kDa) in the infarcted rat brain. *J Nucl Med* 2010;51:1301-9.
184. Veenman L, Gavish M. The peripheral-type benzodiazepine receptor and the cardiovascular system. Implications for drug development. *Pharmacol Ther* 2006;110:503-24.
185. Gaemperli O, Shalhoub J, Owen DR, Lamare F, Johansson S, Fouladi N, Davies AH, Rimoldi OE, Camici PG. Imaging intraplaque inflammation in carotid atherosclerosis with 11C-PK11195 positron emission tomography/computed tomography. *Eur Heart J* 2012;33:1902-10.
186. Yanamoto K, Kumata K, Yamasaki T, Odawara C, Kawamura K, Yui J, Hatori A, Suzuki K, Zhang MR. [18F]FEAC and [18F]FEDAC: Two novel positron emission tomography ligands for peripheral-type benzodiazepine receptor in the brain. *Bioorg Med Chem Lett* 2009;19:1707-10.
187. Yanamoto K, Kumata K, Fujinaga M, Nengaki N, Takei M, Wakizaka H, Hosoi R, Momosaki S, Yamasaki T, Yui J, Kawamura K, Hatori A, Inoue O, Zhang MR. In vivo imaging and quantitative analysis of TSPO in rat peripheral tissues using small-animal PET with [18F]FEDAC. *Nucl Med Biol* 2010;37:853-60.
188. Hatori A, Yui J, Xie L, Kumata K, Yamasaki T, Fujinaga M, Wakizaka H, Ogawa M, Nengaki N, Kawamura K, Wang F, Zhang MR. Utility of translocator protein (18 kDa) as a molecular imaging biomarker to monitor the progression of liver fibrosis. *Sci Rep* 2015;5:17327.
189. Hatori A, Yui J, Yamasaki T, Xie L, Kumata K, Fujinaga M, Yoshida Y, Ogawa M, Nengaki N, Kawamura K, Fukumura T, Zhang MR. PET imaging of lung inflammation with [18F]FEDAC, a radioligand for translocator protein (18 kDa). *PLoS ONE* 2012;7:e45065.
190. Krishnan S, Otaki Y, Doris M, Slipczuk L, Arnsen Y, Rubeaux M, Dey D, Slomka P, Berman DS, Tamarappoo B. Molecular imaging of vulnerable coronary plaque: A pathophysiologic perspective. *J Nucl Med* 2017;58:359-64.
191. Cocker MS, Mc Ardle B, Spence JD, Lum C, Hammond RR, Ongaro DC, McDonald MA, Dekemp RA, Tardif JC, Beanlands RS. Imaging atherosclerosis with hybrid [18F]fluorodeoxyglucose positron emission tomography/computed tomography imaging: What Leonardo da Vinci could not see. *J Nucl Cardiol* 2012;19:1211-25.